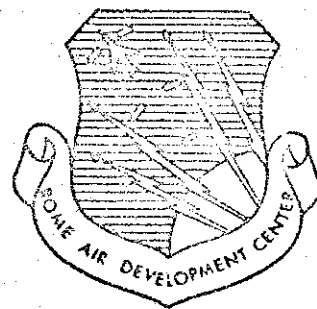


AD-88784

RADC-TR-65-297
Final Report



Note 13

INDUCTIVE STORAGE SWITCH STUDY

TECHNICAL REPORT NO. RADC-TR- 65- 297
December 1965

Techniques Branch
Rome Air Development Center
Research and Technology Division
Air Force Systems Command
Griffiss Air Force Base, New York

CLEARINGHOUSE	
FOR FEDERAL GOVERNMENT	
TECHNICAL REPORTS FILE	
Hardcopy	Microfilm
100	110
APR 1966	

Distribution of this document is unlimited

When US Government drawings, specifications, or other data are used for any purpose other than a definitely related government procurement operation, the government thereby incurs no responsibility nor any obligation whatsoever; and the fact that the government may have formulated, furnished, or in any way supplied the said drawings, specifications, or other data is not to be regarded, by implication or otherwise, as in any manner licensing the holder or any other person or corporation, or conveying any rights or permission to manufacturer, use, or sell any patented invention that may in any way be related thereto.

Do not return this copy. Retain or destroy.

INDUCTIVE STORAGE SWITCH STUDY

Distribution of this document is unlimited

FOREWORD

This final report was prepared by Advanced Kinetics, Inc., 1231 Victoria Street, Costa Mesa, California for the Rome Air Development Center under Contract AF30(602)-3512, Project No. 4506, Task No. 450603.

The following personnel contributed to the work presented in this technical report: Dr. H.P. Furth, Dr. R.W. Waniek, Mr. D.M. Fitzgerald, Mr. T. Emil, Mr. W.L. Lobdell, Mr. P.J. Jarmuz, Mr. J.E. Witsken and Mr. J.G. Koscelnik.

RADC Project Engineer was Frank E. Welker, EMATP.

This report has been reviewed and is approved.

Frank E. Welker

Approved: FRANK E. WELKER
Project Engineer

Alfred W. Parker

Approved: THOMAS S. BOND, JR.
Colonel, USAF
Chief, Surveillance
and Control Division

FOR THE COMMANDER:

Irving J. Babelman

IRVING J. BABELMAN
Chief, Advanced Studies Group

ABSTRACT

An "interrupter" switch was designed and fabricated for use with inductive energy storage devices in pulsed modulator applications. The storage inductor and related circuitry has also been designed keeping in mind the cooling techniques to be employed and the uses of the modulator system. The switch makes use of a low impedance liquid metal - metal contact during the conduction cycle and is opened by a pulsed magnetic field which physically moves the liquid metal away from the solid metal contact.

EVALUATION

INDUCTIVE STORAGE SWITCH STUDY

This effort was an investigation of "interrupter" switching techniques for use with inductive or magnetic field energy storage devices in pulsed modulator operation. The techniques were to be investigated for operation at pulse lengths, pulse repetition frequencies, and pulse energies suitable for use in long range radar systems. The switches developed were to be in a form that could be easily integrated into the total modulator unit and that could function in the cooling environment of the storage element. The fabrication of full scale working models was not anticipated in this effort but the switching techniques under investigation were to be reduced to device concepts.

The contractor established design parameters for an optimum inductive storage system and fabricated a 10 kilojoule inductor for use in evaluating switching techniques. A comparison of cooling liquids such as water, liquid nitrogen, and liquid helium was carried out. In a state-of-the-art cryogenic environment, this study established that the best coolants were water or liquid nitrogen. Of course, a major breakthrough in the development of super-conducting magnets capable of high transient currents could change this and make super cooled devices more useful. The relatively high resistance of plasma arcs makes them inferior to solid or liquid metal contacts in the low impedance inductive storage systems. The "interrupter" switching technique developed was a magnetically opened liquid metal - metal bar contact. The use of relatively high conductivity liquid metals such as liquid sodium in the device and the careful design of the storage element makes room temperature inductive storage systems potentially useful in pulse modulator application. This is especially true where their inherent high energy storage density can be used to advantage.

This effort is part of an investigation of energy storage techniques having higher energy storage densities than is possible with conventional capacitor or electric field systems when used in pulse modulator applications. Both magnetic field and mechanical energy storage systems have higher theoretical energy storage densities than capacitor systems do. Mechanical systems with a rotating mass as the storage element were investigated under Contract AF30(602)-2149 with P.I.B. The preliminary results in this program

indicate that electromechanical or rotating mass storage systems are superior at very long pulse lengths, the magnetic storage systems are superior at the middle pulse lengths and capacitor storage elements are superior at the very short pulse lengths.

Frank E. Welker

FRANK E. WELKER
Project Engineer

TABLE OF CONTENTS

	Page
I) PHYSICAL PRINCIPLES OF INDUCTIVE ENERGY STORAGE.....	1
1) Analysis of Air-Core Inductor.....	4
2) Analysis of Iron-Core Inductor.....	6
II) RELATIVE USEFULNESS OF CAPACITATIVE AND INDUCTIVE ENERGY STORAGE AT HIGH REPETITION RATES AND HIGH LOAD INDUCTANCES.....	9
III) ANALYSIS AND DEVELOPMENT OF BROOKS COILS FOR INDUCTIVE STORAGE.....	12
1) Considerations Regarding Optimum Inductance Coils.....	12
2) Construction of Experimental Energy Storage Inductor.....	14
3) Experimental Studies with IND-1.....	18
IV) EXPERIMENTS ON IRON POWDERS.....	21
1) General Experimental Procedures.....	21
2) Permeability Measurements.....	22
3) Iron Powder Experiments with IND-1.....	27
V) THEORETICAL CONSIDERATIONS ON INDUCTIVE SWITCHING EFFICIENCY.....	32

TABLE OF CONTENTS - (Continued)

	Page
VI) THE INTERRUPTION OF THE INDUCTIVE CIRCUIT.....	39
1) Inductive Discharge Circuits.....	39
2) Problem of Suppression of Interrupter Spark.....	39
VII) MAGNETICALLY ACTUATED SOLID ELEMENT INTERRUPTERS.....	43
1) General Principles.....	43
2) Study of Interrupter Switch Opening-Time.....	45
3) Transfer Experiments with SSI-2 and IND-1.....	47
VIII) MAGNETICALLY ACTIVATED FLUID-METAL INTERRUPTERS.....	52
1) Theoretical Considerations.....	52
2) Studies with Liquid Mercury Interrupter Configuration MSI-1.....	58
3) Studies with Liquid Sodium Interrupter Configuration MSI-2.....	62
IX) CONCLUSIONS.....	66
REFERENCES.....	69

ILLUSTRATIONS - Figures 1 - 36

1) PHYSICAL PRINCIPLES OF INDUCTIVE ENERGY

STORAGE

The energy density stored in magnetic field is

$$W = \frac{1}{4\pi} \int H dB \quad (1)$$

which simplifies to

$$W = \frac{1}{8\pi} \frac{B^2}{\mu} \quad (2)$$

if $\mu H = B$, with constant μ . In ferromagnetic materials, μ is generally not constant, and Eq. (1) then yields considerably lower energy densities for a given storage field B than does Eq. (2). This is illustrated in Fig. 1. Accordingly, when iron is used, the energy should still be stored outside the iron. From Eqs. (1) and (2) we see that the presence of iron always lowers the energy that is stored in a given volume at a given field B . The advantage of using iron lies purely in lengthening the L/R decay-time of the inductive storage facility, thus saving on the charging-power requirement or on the amount of conductor needed in the coil. Since bulk iron powder is relatively cheap, compared with finished conductor windings on a volume-for-volume basis, it makes sense to think of using iron in inductive energy storage facilities.

In order to deduce the optimum amount and shape of iron and conductor, we carry through a generalized analysis, which also includes the case of the pure

air-core coil.

Let the energy be stored outside the iron, in any case. Then Eq. (2) applies, and the total stored energy is

$$E = \int dV \frac{B^2}{8\pi\mu} \quad (3)$$

The flux passing through the coil is

$$\Phi = \int_{A_c} dA \pi \cdot \bar{B} \quad (4)$$

where A_c is the inside coil area and π the unit normal. The power consumption is

$$P = I^2 R \quad (5)$$

where I is the total ampere-turns in the coil and R is the resistance of the coil if it had only one turn.

Now, a rigorously correct relationship is

$$4\pi I = \oint d\ell \frac{B}{\mu} \quad (6)$$

where $d\ell$ is an element of length along a field line, the integral being taken all around a closed loop. Let τ be the decay-time of the stored energy. We define

$$\tau \equiv 2E/P = 4\pi \int dV \frac{B^2}{\mu} / \left\{ \left[\oint d\ell \frac{B}{\mu} \right]^2 R \right. \quad (7)$$

From Eq. (7) we see that if μ is large almost everywhere then τ tends to be very long, and we can afford to economize on conductor material by increasing R . On the other hand, as already noted, this approach gives us less and less E for a given B , and since B is limited to 10-20 kilogauss by the saturation of the iron, we run into the trouble of storing too little energy.

To see where the practical optimum lies, it is convenient to use the following analysis. Let the volume integral in Eq. (3) be divided up:

$$E = \frac{1}{8\pi} \oint d\ell \int_{A(\ell)} dA \frac{B^2}{\mu} \quad (8)$$

where $A(\ell)$ is the effective area of the flux at some point ℓ along a representative field line (see Fig. 2). Let μ and B be approximately constant over A . Using the fact that the flux Φ is constant along ℓ , we then have

$$E = \frac{\Phi}{8\pi} \int d\ell \frac{B}{\mu} \quad (9)$$

$$= \frac{1}{2} \Phi I \quad (10)$$

which we recognize, in fact, as being exactly correct, since $\Phi = LI$ and $E = \frac{1}{2} LI^2$. For τ we then have, of course, $\tau = L/R$.

We now consider two alternatives: air-core coils and coils wound around an iron yoke with an air-gap. In the air-core case, the flux comes from $\Phi = LI$,

so that P and E are proportional. In the iron-core case, a constant saturation flux $\Phi = B_m A_c$ is set up over a wide range of I . Thus, E varies only as $I^{1/2}$ within the current range lying between saturation and quite small values of I . Generally speaking, the iron-core method is most appropriate when DC power is very limited and weight of the inductor is no serious consideration. The air-core method is more appropriate when there is plenty of DC power and one desires to keep down the weight of the inductor.

1) Analysis of Air-Core Inductor

The coil that has the greatest inductance for a given resistance is the Brooks coil shown in Fig. 3. For a single turn, the inductance is

$$\begin{aligned} L &= .0127 d \quad \mu\text{h} \\ &= 12.7 d \quad \text{e.m.u.} \end{aligned} \quad (11)$$

where d is the inside coil diameter. The single-turn resistance for aluminum alloy of twice copper resistivity is

$$\begin{aligned} R &= \frac{8.6}{d} 10^{-5} \quad \Omega \\ &= \frac{8.6}{d} 10^4 \quad \text{e.m.u.} \end{aligned} \quad (12)$$

so that

$$\tau = 1.5 d^2 10^{-4} \quad \text{sec} \quad (13)$$

From Eqs. (5) and (10) we then have simply

$$E = \frac{1}{2} P_T \quad (14)$$

The weight of the coil is

$$M = .82 \tau^{3/2} \text{ tons} \quad (15)$$

so that

$$E = .57 P M^{2/3} \quad (16)$$

A 2-ton aluminum coil will thus require 11 kilowatts to store 10 kilojoules.

This is rather inefficient energy storage, since the mean storage field is low.

To calculate this, we note that

$$L I = A_c B_0 \quad (17)$$

Now $A_c \sim d^2 = 1.2 \cdot 10^4 \text{ cm}^2$ and $I = 120 \text{ kiloamps} = 1.2 \cdot 10^4 \text{ e.m.u.}$,
so that the mean storage field B_0 in the interior of the coil is only 1400 gauss.

The same storage coil could easily withstand 400 times the energy density -- in other words, 4 megajoules storage at 4.4 megawatts charging power. Such a high charging power is not unreasonable if drawn transiently from rotating equipment. Alternatively, one could cut the coil size by using higher power: at 550 kilowatts, one obtains 50 kilojoule storage in a 63 kilogram coil at $B_0 = 18,000$ gauss. This kind of operation is particularly

appropriate if the inductance is charged from a slow capacitor bank, for test purposes, or to make the capacitor energy more rapidly available.

If, however, one needs to remain at low charging powers, then the most economical move is to use a cheap iron-powder core. In that case, B_0 rises to B_m , without expenditure of power. Thus, ϕ becomes multiplied by B_m/B_0 , which is a factor of about 7 in the 1400 gauss example quoted above. From Eq. (10) we then see that the energy storage increases by the same factor B_m/B_0 , without added power needs. In practice, one must take into account the relative cost of conductor and iron, and optimize the proportion.

2) Analysis of Iron-Core Inductor

From Eqs. (5) and (10) we have

$$E = \frac{B_m}{2} A_c \frac{P^{1/2}}{R^{1/2}} \quad (18)$$

which shows right away that this method becomes particularly appropriate for small P . For a coil of cross-section s^2 and diameter d , we have

$$A_c = \frac{\pi}{4} d^2 \quad (19)$$

$$R = \frac{\pi d}{s^2} \eta \quad (20)$$

where η is the resistivity. If the volume of the conductor is

$$V_C = \pi d s^2 \quad (21)$$

and the volume of iron needed to make a nearly complete yoke of cross-section A_C is

$$V_I \sim 3d^3 \quad (22)$$

we can rewrite Eq. (18) as

$$E = .072 \frac{B_m P^{1/2}}{\eta^{1/2}} V_I^{1/3} V_C^{1/2} \quad (23)$$

Next, we optimize V_I relative to V_C . If the cost of iron powder is ϵ times the cost of conductor per unit volume, then let us define

$$V_C^* = V_C + \epsilon V_I \quad (24)$$

so that V_C^* is a measure of the total cost. Maximizing E for constant V_C^* , we find the optimum

$$\epsilon V_I = \frac{2}{5} V_C^* \quad (25)$$

$$V_C = \frac{3}{5} V_C^* \quad (26)$$

The corresponding energy is

$$E = .041 \frac{B_m P^{1/2}}{\eta^{1/2} \epsilon^{1/3}} V_C^{*5/8} \quad (27)$$

For aluminum windings as in the prior example, and for a conservative

$B_m = 10$ kilogauss, we have at $P = 10$ kilowatts $= 10^{11}$ e.m.u.,

$$\begin{aligned} E &= 7.2 \cdot 10^{11} \frac{M^{*5/8}}{\epsilon^{1/8}} \text{ e.m.u.} \\ &= 7.2 \frac{M^{*5/8}}{\epsilon^{1/8}} \text{ kilojoules} \end{aligned} \quad (28)$$

where M^* is the mass of conductor corresponding to V_C^* . Comparing this with the air-core Eq. (16), we see a marked improvement. When $M^* = 2$ tons, $\epsilon = .2$, we now have $E = 23$ kilojoules.

When $M^* = 5$ tons, we have $E = 50$ kilojoules. In that case, the real conductor mass is 3 tons and the iron mass is 30 tons. This amount of iron is not too inconvenient when shipped in modular units and used to fill a box that makes up the yoke. (Use of charging power higher than $P = 10$ kilowatts would allow a mass reduction proportional to $P^{-3/8}$.) For the 5-ton example, we calculate the parameters $d = 120$ cm, $s = 55$ cm.

II) RELATIVE USEFULNESS OF CAPACITATIVE AND INDUCTIVE ENERGY STORAGE AT HIGH REPETITION RATES AND HIGH LOAD INDUCTANCES

Economic studies have been carried out previously¹ for the case of single-pulse operation, comparing the cost of the inductor coil plus charging supply, with the cost of the equivalent capacitor bank and accessories. It is typically found that only at the 100 kilojoule level does the inductive storage begin to become advantageous.

At high repetition rate, the situation is altogether different. The L/R-decay time τ of the storage inductance determines the mass M of the coil (typical example: copper Brooks coil),

$$M = .8 \tau^{3/2} \text{ tons} \quad (1)$$

The requirement on τ is now $\tau \gg \tau_r$, where $1/\tau_r$ is the repetition rate. This contrasts with the single-pulse situation, where $\tau = 2E/P$, and where τ must be made large if the charging power P is to remain moderate. For high-repetition-rate operation, P is fixed at

$$P = E/\tau_r \quad (2)$$

whether capacitive or inductive storage is used. The additional cost for the capacitors themselves is proportional to E , roughly at the rate of \$300 per kilojoule for

a very large bank and \$1000 per kilojoule for a small one. The cost of the inductive storage at very high repetition rate is always limited from below by the mechanical strength of the coil. At a conservative 25 kilogauss storage field, which causes no mechanical or heat-removal problems, one stores 2.5 joules/cm³, corresponding very roughly to \$10 per kilojoule for large facilities, and \$50 for small ones. If τ_r is large enough to set the lower limit on coil size, via $\tau \gg \tau_r$, then the cost follows from Eq. (1), and is given roughly by

$$\$ = 10,000 \tau^{3/2} \quad (3)$$

These various considerations are incorporated in the illustrative diagram of Fig. 4.

These considerations about the cost of the storage facility, however, may not turn out to be of critical importance in the choice of a practical unit. At high repetition rate, the cost of the power source tends to become much greater than that of the storage facility. In that case, the key items in the comparison of capacitors and inductors are: (a) the energetic efficiency of the discharge, and (b) the relative cost of high-voltage and low-voltage charging power.

The energetics of the discharge will tend to favor capacitors, except in unusual situations, or in case a highly efficient interrupter element can be developed. The economics of the charging supply tend to favor the inductive storage.

If the load has high impedance, so that low-current, ultra-high-voltage pulses are called for, the inductive storage is potentially at its best, since it multiplies

the charging voltage, while the capacitive system multiplies the charging current. With suitable design of the interrupter element, the storage inductance can generate any desired voltage directly, without need of an auxiliary transformer. If the interrupter element cannot be designed to tolerate the needed voltage, the transformer feature can be incorporated directly into the storage inductance, thus minimizing stray magnetic energy (Fig. 5).

One notes also that at high repetition rates, where the cost of either inductive or capacitive storage becomes small relative to the cost of the needed power supply, it makes sense to combine the two, placing a shunt capacitor across the load to maximize the efficiency of the interrupter element (Fig. 6). In this way, low-voltage charging of the inductor can be combined with nearly 100% efficiency of energy transfer, as for the capacitor bank. For ultra-high-voltage operation, the shunt capacitor can consist of a series of capacitors with graded potentials, and, due to the transience of high voltage, the corona problem does not become severe.

III) ANALYSIS AND DEVELOPMENT OF BROOKS COILS FOR INDUCTIVE STORAGE

1) Considerations Regarding Optimum Inductance Coils

It is found that for maximum inductance, with a given length of chosen wire, the mean diameter of the turns should be 2.967 times the dimension of the square cross section ($\frac{2a}{c} = 2.967$). However, the maximum is rather flat. For all practical purposes, if this parameter is chosen to be 3, such a coil offers an inductance only 2 parts in 100,000 less than the maximum attainable with the chosen wire length. The inductance of this coil is given by the formula

$$L = .016994 a N^2 \mu h \quad (1)$$

where a is mean radius of turns and N is the total number of turns. However, this formula has a built-in assumption of a completely filled cross-section and a uniform current distribution. The effect of a uniform insulating space between turns and between layers is given by a correction term

$$\Delta L = .004 \pi a N \left[\ln \frac{p}{\delta_1} + .1381 + E \right] \quad (2)$$

where p is the distance between centers of adjacent wires and δ_1 is the diameter of bare wire. E is a constant depending upon the number of layers and number of turns in each layer. E is usually assumed to be .017.

Consequently, the corrected value of the inductance becomes

$$L + \Delta L = \left\{ 1 + (.739/N) [\ln(p/\delta_1) + .155] \right\} L \quad \mu\text{h} \quad (3)$$

While the dependence of the inductance L on the fractional cross-section of conductor λ is seen to be quite weak, the resistance R is, of course, inversely proportional to λ . The resistive decay time τ is then directly proportional to λ , and we have for the stored energy

$$E = \frac{1}{2} P \tau_0 \lambda \quad (4)$$

where τ_0 is the decay time for a coil of $\lambda = 1$. The weight of an air-core Brooks coil (see Eq. 15 in Section I) is now reduced to

$$M = .82 \tau_0^{3/2} \lambda \quad (5)$$

and so we have

$$E = .57 P M^{2/3} \lambda^{1/3} \quad (6)$$

For $\lambda = 1$, we get the most energy stored for a given P and M . For $\lambda < 1$ (hollow tubing) the needed mass goes like $\lambda^{-1/2}$, for fixed P and E .

For an iron-core coil, Eq. (18) of Section I becomes

$$E = \frac{B_m}{2} A_c \frac{P^{1/2}}{R^{1/2}} \lambda^{1/2} \quad (7)$$

$$= .072 \frac{B_m P^{1/2}}{\pi^{1/2}} V_1^{1/3} V_c^{2/3} \quad (8)$$

so that the magnitude of λ drops out. This just means that with an iron-core of a given size it does not matter how the conductor cross section is distributed inside the core window.

The relations that exist between the principal dimensions of these optimized storage coils are illustrated in Fig. 3.

2) Construction of Experimental Energy Storage Inductor

A small experimental inductor was developed with a threefold objective:

- i) To provide an experimental inductor at 10 - 20 kilojoules storage, intended for studying the discharge and interruption problems. Powering is by a capacitor bank, discharging in 1 millisecond into the inductor.
- ii) To study the effectiveness and optimum shape of iron cores, using the capacitor bank, or the liquid nitrogen plus DC power.
- iii) To study the effectiveness of liquid nitrogen cooling, charging the inductance from a DC power supply.

The inductor weighs 50 kilograms and is wound of copper conductor, with a small hole for circulating water or liquid nitrogen. The inductance is

$$L = .23 N^2 \mu h \quad (9)$$

where N is the number of turns.

The resistance is

$$R = 2.3 N^2 10^{-8} \Omega \quad (10)$$

The decay constant is $\tau = 100$ millisecon. The dimension "C" is 9 cm, so that the diameter is 18 cm. The mean storage field is 15 kilogauss.

For charging from a capacitor bank of 10 kilojoules energy at 10 kilovolts, with a charging time of 1 millisecon and a current of 3 kiloamps, we need $N = 90$ turns. The coil is made of 10 windings of 9 turns each, with their ends exposed so that they can be connected in various ways to step up the discharge current, or to allow more rapid charging by the capacitor bank.

For DC charging at 3 kiloamp peak, it would require at least 200 kilowatts to achieve 10 kilojoules storage. With liquid-nitrogen cooling, this can be cut to 24 kilowatts. The cooling down costs \$7, and the operation costs \$164 per hour. Each charging operation should only take about 4 seconds, so that the cost per pulse is only 16¢.

Since the mean storage field at 10 kilojoules is 15 kilogauss, iron is not helpful. The point here is that iron becomes economical only in the case of low charging power, i.e., for larger coils and lower storage fields. What we can do, however, is to study the effect of iron, letting the storage energy drop, for example, to 1 kilojoule, while the DC power drops to 20 kilowatts at room temperature, or to 2.0 kilowatts at LN temperature. For

convenience, the iron-core coil can also be pulsed on by capacitor bank. The core can be filled with iron powder conveniently contained in plastic bags, which are then taped together to approximate the desired configuration. Table I presents a parametric study for the storage inductor for two cases of $\lambda = 0.31$ and $\lambda = 1$ and two conductor materials, copper and aluminum. The geometry outlined in the first column was selected for the first experimental inductor, IND-1.

TABLE I

Geometry	Material	λ	Inductance (mH)	Quality Factor (Q)
IND-1	Copper	0.31	1.5	100
IND-2	Aluminum	0.31	1.5	100
IND-3	Copper	1.0	1.5	100
IND-4	Aluminum	1.0	1.5	100
IND-5	Copper	0.31	1.5	100
IND-6	Aluminum	0.31	1.5	100
IND-7	Copper	1.0	1.5	100
IND-8	Aluminum	1.0	1.5	100

TABLE I

	COPPER TUBE	ALUMINUM TUBE	COPPER ROD	ALUMINUM ROD
Current	3900 A	3900 A	3900 A	3900 A
Inductance	2.55 mh	2.55 mh	2.55 mh	2.55 mh
Stored Energy	19.4 kj	19.4 kj	19.4 kj	19.4 kj
Length of Conductor	370 feet	370 feet	370 feet	370 feet
Weight of Conductor	53.5 lbs.	16.7 lbs.	157 lbs.	49.5 lbs.
Room Temp. Resistance	72 mΩ	108 mΩ	26 mΩ	39 mΩ
λ Factor	0.31	0.31	1	1
LN Temp. Resistance	7.66 mΩ	10.8 mΩ	2.75 mΩ	3.9 mΩ
Cool-down Requirements	11 liters	7.5 liters	32.5 liters	22.3 liters
Cool-down Expense	\$3.30	\$2.5	\$9.75	\$6.7
Heat Generated at Room Temp.	1100 kw	1640 kw	396 kw	592 kw
Heat Generated at LN Temp.	117 kw	164 kw	42 kw	59.2 kw
Corresponding LN Consumption	2620 liters/hr.	3680 liters/hr.	940 liters/hr.	1320 liters/hr.
Operating Expense at LN Temp.	\$800/hr.	\$1100/hr.	\$282/hr.	\$398/hr.

3) Experimental Studies with IND-1

a) Measurements of IND-1 Electrical Parameters

To determine the electrical parameters of the inductor IND-1, the ends of the coil were clamped securely with aluminum blocks to the ignitron mounting plate of an 800 μf , 4 kv capacitor bank. The bank was charged to the desired voltage and the ignitrons were then triggered shorting the capacitors into IND-1. The resulting discharge was observed with a high voltage probe across the coil and a Rogowski loop around the conductor. Pictures of the oscilloscope traces furnished the data required for calculation of maximum coil current, coil inductance, coil resistance, and efficiency for energy transfer. The analyzed data provided the following results:

	<u>Measured Parameters</u>	<u>Computed Parameters</u>
Inductance	2.56×10^{-3} H	2.55×10^{-3} H
Resistance (room temp.)	0.097 ohm	0.075 ohm
Current (at 1 kv, 800 μf)	512 A	542 A
(at 2 kv, 800 μf)	1024 A	1084 A
Transfer Energy Efficiency		
(1 kv)	90%	94%
(2 kv)	90%	94%

The computed current values were obtained by means of

$$I_p = \frac{V}{L \left(\frac{1}{LC} - \frac{R^2}{4L^2} \right)^{1/2}} \exp \left(-\frac{R}{L} t \right) \quad (11)$$

using the measured parameters, as listed, and $t = \tau_r = 2$ msec.

b) Field Scans of IND-1 Storage Coil

To determine the magnetic field configuration of the IND-1 storage coil, a field pick-up probe of $A_n = 3.945 \text{ cm}^2$ was mounted on a stable scanning device which could be moved along three perpendicular directions. With the scanning device in place over the storage coil, the capacitor bank (800 μf at 4 kv, 6,400 joule) was discharged through the coil. Each field measurement was made under identical conditions so as to obtain the field profile of the coil.

The integrated output of the probe was displayed on an oscilloscope and the field values were then calculated using the recorded trace and the known parameters of the probe.

Field scans were made in the following manner:

Vertical

- a) Flux density along axis of IND-1 storage coil (see Fig. 7a)
- b) Flux density along inside wall of IND-1 storage coil parallel to coil axis (see Fig. 7b)

- c) Flux density along outer wall of IND-1 storage coil parallel to coil axis (see Fig. 7c)

Horizontal

- a) Flux density of IND-1 storage coil in the equatorial plane of the coil (see Fig. 7d)

IV) EXPERIMENTS ON IRON POWDERS

1) General Experimental Procedures

The object is to determine the optimum shape of the core, and the performance of various powders. The μ can be measured directly on small samples by using the standard torsion-balance technique, or by embedding different-shaped magnetic probes. This is based on the familiar continuity of B_{normal} and $H_{\text{tangential}}$.

To determine the performance of powder cores in the inductive coil, it is convenient to make measurements on the circuit instead of on the medium. We want to measure both dI/dt and also V across the coil, using a fast enough oscillation so that R is small compared with $L\omega$. Then

$$V = I(dL/dt) + L(dI/dt) \quad (1)$$

and we can determine how both I and L vary. We now define

$$h = I \quad (2)$$

$$b = IL/L_0 \quad (3)$$

$$\mu_c = b/h \quad (4)$$

where L_0 is the coil inductance in the absence of iron. Then $\mu_c = 1$ in the absence of iron. We also have

$$E = \int dt IV \quad (5)$$

$$= \int d(LI)I \quad (6)$$

$$E = L_0 \int h db \quad (7)$$

which we want to maximize for a given h . This situation corresponds exactly to the usual expression

$$E = \int dV \int H dB \quad (8)$$

As discussed previously, we must avoid having b reach its maximum value for too small an h . This can be accomplished by introducing air-gaps, as needed, into the iron core.

To measure b , we just integrate V across the coil. To measure h , we integrate dI/dt . To obtain the normalizing factor L_0 , we first run the measurements with no iron in the coil.

2) Permeability Measurements

Permeability measurements were conducted on the following types of powders available from Hoeganaes Sponge Iron Corporation, Riverton, New Jersey.

<u>Type</u>	<u>Composition</u>	<u>Density (g/cm³) (not compacted)</u>
MH-100	98.8% Fe	2.45
EP-1024	99.0% Fe	2.55
MH-300	98.0% Fe, 0.2% SiO ₂	2.80
Grade B	96.5% Fe, 0.3% C	2.40

The values of μ for these powders varies considerably depending on the "packing factor", i.e., the ratio of the volume of the metal to the volume filled by the powder. The graph of Fig. 8 illustrates this phenomenon for a typical iron powder.

The cost of the iron powder is relatively small. For example, the cost of one or more tons of Grade B powder is \$.0925 per pound.

The method for the determination of the powder permeabilities involved the use of three test coils with different inductances. The parameters of the coils are given as follows:

Coil	A	B	C
Layers	1	2	3
Number of Turns	262	655	933
Length (cm)	7.19	7.80	7.80
Radius (cm)	0.91	0.92	0.93
Inductance (μ h)	360	1500	3375
Resistance (ohms)	5.98	12.98	19.53

The coils were formed by winding wire Type AWG 30 on a graduated test tube. After obtaining the coil parameters, a controlled volume of the powder under investigation is poured into the tube and into a beaker which encases the tube. Since the mass of the powder is also determined,

the density is accurately known. During the experiment the powders are not densified in any way. The density values of the powders at the time of the permeability measurements are given in Table II.

With the powder in and about the coil, an inductance measurement is made and recorded. Employing the inductance formula for a coil,

$$L = \mu \frac{4\pi^2 r^2 N^2}{\ell} \quad (9)$$

where r is the radius of the coil, N is the number of turns, and ℓ is the length of the windings, it is possible to determine the permeability, μ_p , of the powder from the relationship

$$\mu_p = \mu_a \frac{L_p}{L_a} \quad (10)$$

where μ_a and L_a are the permeability of air and inductance of the coil in air, respectively, and L_p is the measured inductance of the coil in the powder.

During the measurements of the inductances of the various powders, a vacuum tube voltmeter is placed in the circuit so that the voltage reading of the coil can be obtained. Using the voltage obtained, it is possible to determine the value of the current in the coil from the relationship

$$I = V/R \quad (11)$$

where R is the measured resistance of the coil.

Utilizing the expression

$$H = NI/l \quad (12)$$

we may readily determine the value of the magnetic field intensity, H .

The flux density is obtained from the relationship

$$\mu = B/H \quad (13)$$

The results obtained are summarized in Table II. Figure 9(a) illustrates the relationship of the flux density and the magnetic field intensity for the various powders. Included in this figure are the results from each of the experimental coils. Figure 9(b) expresses the permeability of the powders as a function of excitation current.

TABLE II

COIL A

POWDER	DENSITY g/cm ³	L mh	V v	I amp	μ gauss/Oe	H Oe	B gauss
MH-100	2.45	1.582	0.13	0.022	4.52	0.080	0.362
EP-1024	2.72	1.640	0.13	0.022	4.69	0.080	0.375
MH-300	2.63	1.390	0.11	0.018	3.97	0.066	0.262
Grade B	2.69	1.260	0.09	0.015	3.60	0.055	0.198

COIL B

MH-100	2.45	7.020	0.86	0.66	4.67	0.55	2.57
EP-1024	2.70	7.042	0.90	0.69	4.69	0.58	2.72
MH-300	2.64	6.375	0.78	0.60	4.52	0.50	2.13
Grade B	2.64	5.345	0.64	0.49	3.56	0.41	1.46

COIL C

MH-100	2.45	15.53	1.96	0.100	4.60	1.20	5.52
EP-1024	2.75	16.10	2.00	0.102	4.77	1.22	5.82
MH-300	2.64	13.53	1.70	0.087	4.01	1.04	4.17
Grade B	2.69	11.94	1.45	0.074	3.54	0.89	3.15

3) Iron Powder Experiments with IND-1

a) Uncompacted Powders

The following section illustrates the inductance changes involved in placing iron powder packed in polyethylene bags in various configurations in and about the IND-1 Brooks coil.

The inductance measurements utilizing the iron powders are obtained by means of a one-turn field pick-up coil by which it is possible to measure the current change with respect to time, dI/dt . This value, together with the expression

$$L = \tau^2/4\pi^2 C \quad (14)$$

where τ is the period in seconds and C is the capacitance in farads, determines the inductance, L .

In Table III is presented a schematic of the configurations of iron powder used in the experimental evaluation and the observed inductance increases, ΔL , where

$$\Delta L = (L_p - L_o)/L_o \quad (15)$$

It will be observed that the greatest inductance increase occurs for configuration D in which the polyethylene bags of powder are placed throughout the entire core of the coil.

Results with other configurations may be summarized as

follows:

<u>Configuration</u>	<u>$\Delta L = (L_p - L_o) / L_o$</u>
D-1	54%
H	65%
J	75%
K	81%

D-1: Powder packages are arranged similarly to Configuration D except that packages are lengthwise in the vertical direction permitting a greater volume of powder to be placed in the center of the coil.



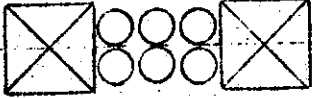
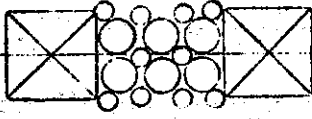

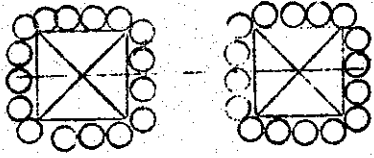
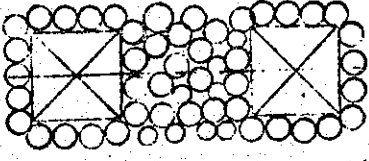
H: Powder packages arranged with center fully packed as in D-1 and with opposite continuous rings of packages.

J: Center of coil as in D-1 with two continuous opposite pairs of rings at $\sim 90^\circ$.

K: Center of coil as in D-1 but with three continuous opposite pairs of rings at $\sim 60^\circ$.

IRON POWDER CONFIGURATIONS

TABLE III

<p>Configuration A</p>  <p>$L_o = 1.70 \text{ mh}$</p>	
<p style="text-align: center;">Configuration B</p>  <p>Three bags aligned along equatorial plane</p> <p>$L_p = 1.80 \text{ mh}$ $\Delta L = 6\%$</p>	<p style="text-align: center;">Configuration C</p>  <p>Six bags aligned along equatorial plane</p> <p>$L_p = 1.74 \text{ mh}$ $\Delta L = 2\%$</p>
<p style="text-align: center;">Configuration D</p>  <p>Center of coil completely filled with powder packages</p> <p>$L_p = 2.11 \text{ mh}$ $\Delta L = 24\%$</p>	<p style="text-align: center;">Configuration E</p>  <p>Powder packages arranged in continuous ring about coil</p> <p>$L_p = 1.91 \text{ mh}$ $\Delta L = 12\%$</p>
<p style="text-align: center;">Configuration F</p>  <p>Powder packages in opposite continuous rings</p> <p>$L_p = 1.94 \text{ mh}$ $\Delta L = 14\%$</p>	<p style="text-align: center;">Configuration G</p>  <p>Opposite continuous rings joined by powder packages</p> <p>$L_p = 2.07 \text{ mh}$ $\Delta L = 22\%$</p>

b) Compacted Powders

Various grades of powdered iron were compacted hydraulically at different pressures in the range of 10 - 20 tons. The degree of densification obtained for the various grades of powder as a function of the applied pressure is illustrated in Fig. 10. Measurements indicated an increase in the permeability of the compacted samples by a factor of two over the non-densified state.

The powders were compacted into small cylinders of axial length ≈ 1.5 " and radius ≈ 0.75 ". Approximately 50 of these samples were placed in the core of IND-1. The geometry of the samples precluded a complete packing of the core. Consequently, a total air gap of $\approx 35\%$ remained in IND-1. An inductance rise, ΔL , of 34% over the air inductance, L_0 , was observed with this configuration. The placing of small undensified powder packages around the perimeter of the core produced an inductance rise of 49%. This latter configuration still possessed an air gap of $\approx 25\%$ in the regions between the individual compacted samples. These measurements are somewhat less than the observed incremental inductance rise, ΔL , for the undensified packing of the entire core volume (see Configuration K). Consequently, with optimized packing of the compacted billets, i.e., with the elimination of the 25% air gap, an inductance rise far in excess of the value

obtained for the uncompacted configuration would result.

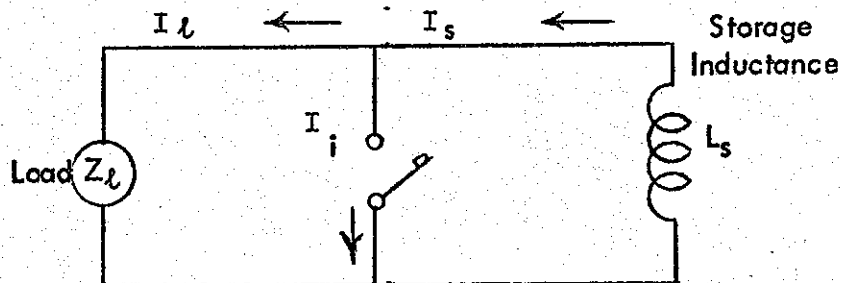
From the above considerations, it is apparent that a more complete optimization of the inductance rise may be obtained by the adoption of two measures.

One plan would be to select a more appropriate cross section for the compacted samples so as to increase the percentage of iron in the core volume. It is felt at this time that compaction in the form of prisms would offer a much more effective method for filling the center of IND-1.

A second measure would be the application of greater pressure to the samples, thus increasing the packing factor and, consequently, the permeability of the sample.

V) THEORETICAL CONSIDERATIONS ON INDUCTIVE SWITCHING EFFICIENCY

We treat here the standard circuit for discharging a storage inductance:



We will confine ourselves to a dissipative type of interrupter (as distinct from capacitative), and we will calculate the energetic efficiency of the circuit for the most general type of load impedance, including time-varying resistance, inductance, etc.

At time $t = 0$, we have

$$\begin{aligned} I_L &= 0 \\ I_i &= I_S = I_0 \end{aligned} \quad (1)$$

while, at time $t = \tau$, where the interrupter is fully open, we have

$$\begin{aligned} I_L &= I_S = I_1 \\ I_i &= 0 \end{aligned} \quad (2)$$

If the initial energy in the storage inductance $L_s = E_0$, then the amounts of energy that have gone into the load and interrupter, and the remaining energy in the source are given by

$$E_L = \int_0^T dt V I_L \quad (3)$$

$$E_i = \int_0^T dt V I_i \quad (4)$$

$$E_s = E_0 - \int_0^T dt V I_s \quad (5)$$

We note that the voltage $-V$ across the source can be written

$$-V = L_s \frac{dI_s}{dt} \quad (6)$$

so that

$$I_s = I_0 - \frac{\phi}{L_s} \quad (7)$$

where

$$\phi = \int_0^T dt V \quad (8)$$

We also have

$$I_L = I_s - I_i \quad (9)$$

Using Eqs. (7) and (9) we can write (4) in the form

$$E_i = \int_0^T dt V \left\{ I_0 - I_L - \frac{\phi}{L_s} \right\} \quad (10)$$

From (2) and (7) we have

$$I_0 = I_1 + \frac{\Phi_1}{L_s}$$

where Φ_1 is the value of Φ at $t = \tau$.

Thus, Eq. (10) becomes

$$E_i = \int_0^\tau dt \frac{d\Phi}{dt} \left\{ I_1 - I_L + \frac{1}{L_s} (\Phi_1 - \Phi) \right\} \quad (11)$$

Finally we write (3) and (11) in the form

$$E_L = \int_0^{\Phi_1} d\Phi I_L \quad (12)$$

$$E_i = \Phi_1 I_1 - \int_0^{\Phi_1} d\Phi I_L + \frac{1}{2} \frac{\Phi_1^2}{L_s} \quad (13)$$

From this result we see that the efficiency

$$\epsilon = E_L / (E_L + E_i) \quad (14)$$

becomes optimal when the third term on the right in Eq. (13) is small, i.e.,

when

$$I_1 \gg \frac{1}{2} \frac{\Phi_1}{L_s} = \frac{1}{2} (I_0 - I_1) \quad (15)$$

so that only a small fraction of the stored energy is extracted on a given pulse.

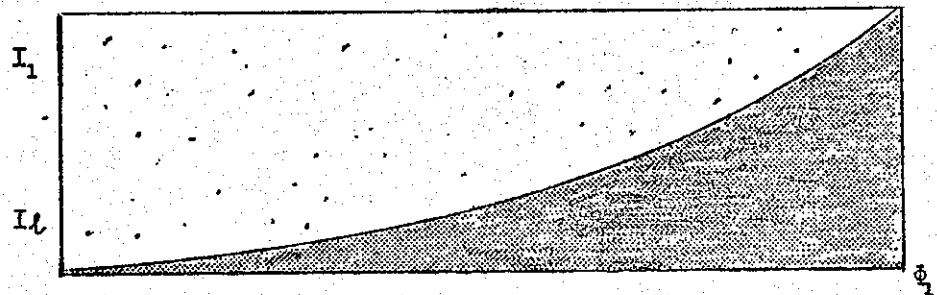
Concentrating for the moment on this regime, we then have left:

$$E_l = \int_0^{\Phi_1} d\Phi I_l$$

$$E_i = \Phi_1 I_1 - \int_0^{\Phi_1} d\Phi I_l$$

This shows that the efficiency depends basically on the $\Phi - I_l$ relationship for the load, that is, on the load impedance and its time-dependence.

If the load impedance V/I_l is initially high and then drops off, as for an inductive load, we have typically the following situation



where the shaded area represents E_l , while the lightly dotted area represents E_i . Specifically, if the load is a constant inductance L_l , we have

$$L_l \frac{dI_l}{dt} = V \quad (16)$$

$$I_l = \Phi / L_l \quad (17)$$

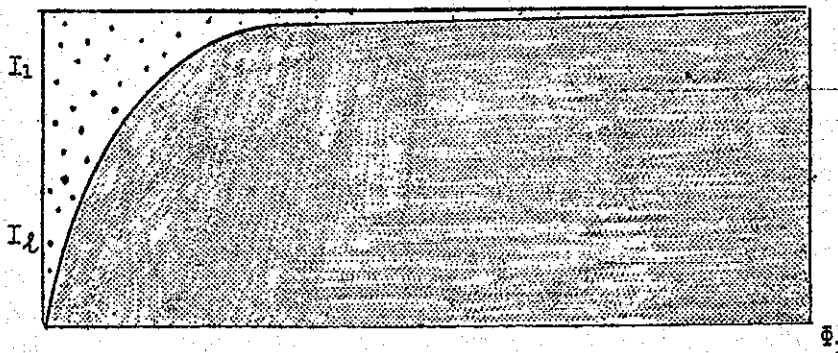
In that case we get $E_l = E_i$ and $\epsilon = 1/2$.

If the load impedance is a constant resistance, R_L , we have

$$R_L I_L = V \quad (18)$$

$$I_L = \frac{1}{R_L} \frac{d\Phi}{dt} \quad (19)$$

In that case, we are free to control the relation between I_L and Φ , simply by the time-history of the impedance in the interrupter. Specifically, we should try to interrupt as quickly as possible, so as to obtain the type of result illustrated here:



In this case there is a continued flow of energy from the inductive source to the resistive load, after the interrupter is open. Hence, another way of describing the situation is to look back at Eq. (13), let the $I_L - \Phi$ relationship be simply

$$I_L = \Phi/R_L \tau \quad , \quad 0 \leq t \leq \tau \quad (20)$$

$$= I_1 \quad , \quad t = \tau$$

$$I_S \quad , \quad \tau \leq t \quad (21)$$

and to obtain

$$\begin{aligned}
 E_i &= \frac{1}{2} \bar{\phi}_1^2 \left(\frac{1}{R_L \tau} + \frac{1}{L_s} \right) \\
 &= \frac{1}{2} R_L \tau I_1^2 \left(1 + \frac{R_L \tau}{L_s} \right)
 \end{aligned} \tag{22}$$

The energy transferred to the load during the time τ is only

$$E_{Ll} = \frac{1}{2} \frac{\bar{\phi}_1^2}{R_L \tau} = \frac{1}{2} R_L \tau I_1^2 \tag{23}$$

but thereafter the energy $\frac{1}{2} L_s I_1^2$ remaining in L_s is transferred in addition.

Thus the net efficiency is

$$\begin{aligned}
 \epsilon &= \frac{R_L \tau + L_s}{R_L \tau + L_s + R_L \tau \left(1 + \frac{R_L \tau}{L_s} \right)} \\
 &= \frac{1}{1 + (R_L \tau / L_s)}
 \end{aligned} \tag{24}$$

which again leads to the previous result that the interruption time should be as short as possible.

If the load impedance is capacitive (or involves an inductance that increases strongly with time) things are still more favorable, because I_L necessarily becomes large before $\bar{\phi}$ does. We then have

$$I_L = \frac{1}{C_L} \frac{d^2 \bar{\phi}}{dt^2} \tag{25}$$

which leads naturally to patterns like that of the second picture. If, for simplicity, we adopt the model

$$I_L = \phi / C_L \tau^2, \quad 0 \leq t \leq \tau \quad (26)$$

$$= I_1, \quad t = \tau$$

$$= I_s, \quad \tau \leq t \quad (27)$$

We can follow the same procedure as for R_L and obtain

$$\epsilon = \frac{1}{1 + (C_L \tau^2 / L_s)} \quad (28)$$

For short interrupter times, the efficiency becomes very high.

VI) THE INTERRUPTION OF THE INDUCTIVE CIRCUIT

1) Inductive Discharge Circuits

A study was conducted to analyze the circuit configurations of interest and their problems and merits. The most suitable circuit would seem to be the one given in Fig. 11(a). When the interrupter is opened, only the voltage $L_s I_0 / \tau_r$ will appear across the DC source, where L_s is its inductance and τ_r is the time for decay of the current in the storage inductance. Even this voltage can be kept as small as desired by using a shunt capacitor C_2 and/or a nonlinear resistor R . The one end of the load remains grounded during the interrupter action. The storage coil will tend to float up to the voltage $L_s I_0 / \tau_r$, but that is not much of a problem.

Notice that the alternative circuit in Fig. 11(b) actually causes a larger voltage $L_s I_0 / \tau_i$ to appear across the DC source during interrupter action in the time τ_i , because the current I_0 initially flowing in the source is suddenly cut off completely.

2) Problem of Suppression of Interrupter Spark

If the load is primarily resistive, then maximum energetic efficiency is achieved by opening the interrupter as quickly as possible. However, the residual inductance L_L in the load will give rise to a voltage $I L_L / \tau_i$ across the interrupter, which becomes large for small interruption time τ_i .

This difficulty can be compensated for by means of a small non-inductive shunt capacitor C_1 . The appropriate magnitude of C_1 is obtained from

$$C_1 I \tau_i = V_{\max} \quad (1)$$

where V_{\max} is the maximum desired voltage during interruption. If τ_i is much less than the resistive energy-extraction time τ_r from the storage inductance, then the energy-rating of C_1 can be much smaller than the total energy transferred.

A second important element in spark-suppression is the proper design and operation of the interrupter itself. If the interrupter makes use of a strong magnetic field, as in Fig. 12, then the cross-field arc between the fixed ring electrode A and the movable disk electrode C is forced to rotate about the axis, creating a back-voltage. The acceleration process for the arc plasma is described by

$$\rho \frac{d\vec{v}}{dt} = \vec{j} \times \vec{B} \quad (2)$$

where ρ is the plasma mass density and \vec{j} and \vec{B} are the current density and magnetic field. The electric field making the back-voltage is given by

$$\vec{E} + \vec{v} \times \vec{B}/c = 0 \quad (3)$$

If the plasma density is low, then Eq. (2) shows that the arc is immediately

accelerated to a high velocity, so that a large back-voltage develops according to Eq. (3), thus holding off the further flow of current in the interrupter. If the plasma density is high, and if neutral gas is being continuously swept into it, as would be the case at atmospheric pressure, then a large current can flow according to Eq. (2), without producing a high plasma velocity or a marked back-voltage. In the latter case, the integrated current and total heating of the element C may be very large.

To get some specific numbers, we may treat the plasma between elements C and A as though it were a capacitative element, with a dielectric constant

$$K = 1 + \frac{4\pi\rho c^2}{B^2} \quad (4)$$

and then apply the usual geometric relation for a two-plate capacitor.

For a gap z between A and C, we get

$$C_i = K \frac{z}{2} \log(r_2/r_1) \quad (5)$$

where C_i is the effective capacity of the plasma, and r_1 and r_2 are the inner and outer radii of the ring electrode A. If the mass density ρ of the plasma is large, then K is large and C_i is large, and then there can be a considerable current flow through C_i . Conversely, if ρ is small, there can be only a small current flow.

Extensive experiments have been done on the back-voltage phenomenon, both at low density² and atmospheric density³. At low density, and with a well-localized plasma, back-voltages of up to 20 kv have been obtained⁴. However, the actual realization of such high voltage requires extreme care in the placement of insulators, otherwise the discharge will cross the magnetic field lines at the insulator surface, and the advantage of the back-voltage in the volume is then lost. When using interrupters of small size and simple construction, it may be most practical to dispense with the back-voltage effect, and use high gas pressure, relying on the ordinary high-pressure inhibition of breakdown, rather than on the magnetic-field inhibition.

VII) MAGNETICALLY ACTUATED SOLID ELEMENT INTERRUPTERS

1) General Principles

A strong pulsed magnetic field can serve simultaneously to interrupt a mechanical contact and to suppress the resultant arcing. The basic design is illustrated in Fig. 13. In the "closed" position of Fig. 13(a), a metal disk anvil makes contact with a contactor embedded in a magnet coil. When the coil field is pulsed on, the magnetic pressure against the anvil disk moves it upward and breaks the contact (Fig. 13b). At the same time, the magnetic field appearing between the contactor and the anvil raises the impedance of the arc. Particularly when the device is operated in vacuum the current flowing between the contactor and the anvil, across the magnetic field, accelerates the plasma in the $\vec{i} \times \vec{B}$ direction, and creates a back-voltage that greatly raises the impedance. In general, the current in such discharges tends to be diverted along the magnetic field to the nearest insulating surface, where it breaks down across the magnetic field if the voltage becomes excessive.

The problems in developing an interrupter of this kind are:

- i) The size must be sufficiently small so that the kinetic energy of the anvil plus the magnetic energy of the coil, represent a small fraction of the inductive storage energy. Since the present study

is aimed at a range of energies, from 100 to 50,000 joules, we will be interested in studying a wide range of interrupter sizes. If, for a start, 10% of the energy can be used in the interrupter mechanism, then in the 50,000 joule case, a kinetic energy of 2500 joules will be appropriate for the anvil. For example, at the attainable velocity of 10^4 cm/sec, this means a weight of 500 grams for the anvil. For a 500 joule storage, the anvil should weigh 5 grams. Both of these numbers appear reasonable in terms of practical devices.

- ii) The interrupter mechanism must be cooled, in the case of high repetition rate. The greatest instantaneous heat load is on the anvil, whose mass is restricted. The best cooling procedure is probably to cool the stationary contactor and press the anvil firmly against it between pulses. The size of the interrupter mechanism can be increased, in case of severe heat load, by reducing the opening velocity, and thus increasing the opening time.
- iii) The plasma behavior after interruption must be studied, with a view to avoiding breakdown along insulators supporting the coil. The voltage obtainable will be limited, and this in turn sets a lower limit on the attainable opening time.

iv) The simultaneous interruption of several contacts made by the same disk should be studied, since this is one important technique for stepping up the output current of the inductor device.

2) Study of Interrupter Switch Opening-Time

A single-shot interrupter switch (SSI-1) composed basically of two copper clamps for holding a metal ring-disk in place over a spirally-wound pancake shaped coil (RG-58 teflon-covered center conductor) was tested for opening time as a function of energy input to the coil (see Fig. 14).

A 2 μ f capacitor, charged to various voltages, was discharged through the interrupter coil. The resulting field produced in the interrupter coil (see Fig. 15) then reacted with the metal-ring disk in such a manner as to force the ring-disk upward and out from under the edges of the two copper clamps, thus breaking contact between the clamps.

Velocities imparted to an 11 gram copper ring have been as high as 150 meters/sec. Velocities were measured by using a stroboscope, and a photograph produced by this means is shown in Fig. 16. Typical results of the velocity versus energy curves for two hollow copper rings is included as Fig. 17.

By placing the combination of a battery in series with a resistor across the clamps, the opening of the switch resulted in a voltage appearing across the clamps. The voltage across the clamps was observed with a 10:1 voltage

probe and an oscilloscope. In addition to the clamp voltage, a field pick-up coil in the vicinity of the interrupter coil allowed the determination of the triggering sequence. The inertial opening time of the switch was taken as the time interval between triggering of the interrupter coil to the time when voltage appeared across the clamps. Obviously, there are two time intervals involved in the inertial opening time described here. The first time interval is the time from actuation of the interrupter coil to the time when contact separation starts and the second time interval is from the starting of metallic separation to the time when current stops flowing in the interrupter clamps. With SSI-1, sporadic break-make opening was observed on some shots before complete metallic separation occurred. The triggering sequence was displayed on the same oscilloscope trace (A-B input) for ease of determining opening time. The best opening time was obtained with an aluminum ring-disk weighing .06 grams. With an energy input to the interrupter coil of 16 joules, the interrupter switch opened in about 17 μ sec. With a copper ring-disk weighing .24 grams, the best opening time was about 170 μ sec for an energy input of 16 joules. The opening time versus energy input is displayed in Fig. 18 for both the copper and aluminum ring-disks.

3) Transfer Experiments with SSI-2 and IND-1

A second and more advanced interrupter, the SSI-2, was developed to conduct exploratory tests on the single shot mechanism of energy transfer (see Fig. 19). Mercury-wetted electrodes were used to produce contact resistance in the low milliohm range.

Initial tests showed opening times of approximately 20 - 30 μ sec without load. This was achieved by discharging 240 joules (9 kv - 6 μ f) into the SSI-2 coil with a risetime of approximately 20 μ sec and using a 25 gram aluminum shaped ring.

The circuit in Fig. 20 was used to study energy transfer from the inductive storage device, the IND-1, into the load. An ignitron crowbar disconnects the charging capacitors from the IND-1 when maximum current is flowing, then, with the load, SSI-2 and a capacitor in parallel, the SSI-2 is fired, diverting the current through the load.

The loads used were made of .041" diameter music wire with resistances of .061 Ω , .160 Ω , .236 Ω , and .500 Ω , and with corresponding measured inductances at 1 kc of 3 μ h, 5.8 μ h, 8.8 μ h and 18.2 μ h.

Shots taken using no shunt capacitor and capacitances of 2 μ f, 15 μ f and 100 μ f show that the change in capacitances varies the length of the arc across the SSI-2, but the effect is so small as to be masked by other factors, i.e., the exact positioning of the ring and the inductance of the SSI-2

itself. Clearly, much larger values of C would be needed to affect the voltage across the arc, on the order of $Q/V \sim (10^3 \text{ amp} \cdot 10^{-3} \text{ sec})/10^2 \text{ v} \approx 10 \text{ mf}$.

Using relatively small loads, as we have been doing, we must realize that the energy dissipated in the IND-1 and the remaining circuitry is a significant portion of the total energy in the circuit. In fact, "perfect" transfers into loads of $.061\Omega$, $.160\Omega$, $.236\Omega$ and $.500\Omega$ consist of 32%, 55%, 65% and 80%, respectively, of the total energy stored in IND-1.

In all shots the IND-1 was energized to 370 joules before interruption. Also, in each case, oscillographs were taken of

- 1) dI/dt in the SSI-2,
- 2) dI/dt in the IND-1,
- 3) current in the IND-1,
- 4) the voltage across the load.

With all these variables under observation, there are several ways of calculating the energy transferred to the load. The method used may be described by the following procedure:

$$E = \int V^2/R dt \quad (1)$$

where R, the load resistance, is a function of the energy already transferred

$$R = R_0 \left(1 + \frac{kE}{Mc} \right) \quad (2)$$

M is the mass of the load, c is the specific heat and k is the coefficient of resistivity.

From these equations we have

$$dE/dt = (V^2/R_0) / (1 + \frac{kE}{Mc}) \quad (3)$$

or

$$\int_0^E (1 + \frac{kE}{Mc}) dE = \int_0^t V^2/R_0 dt \quad (4)$$

$$(kE^2/2Mc) + E = \int_0^t V^2/R_0 dt \quad (5)$$

The solution to this quadratic is

$$E = Mc/k \left\{ \left(1 + \frac{2k}{Mc} \int_0^t V^2/R_0 dt \right)^{1/2} - 1 \right\} \quad (6)$$

Arcing is taking place in all cases when attempting interruption with all three of the higher resistance loads. The energy dissipated in the arc is an appreciable fraction of the total energy, hence the relatively low values in the "% of perfect transfer" columns (see Table IV).

Even under relatively high vacuum conditions, enough heat is apparently liberated to vaporize the insulation (epoxy) around the electrodes and even small portions of the ring and electrodes, thus producing transiently an atmosphere where an arc can occur. When interrupting the circuit, pressure is observed to go from $< 10^{-4}$ Torr to $\sim 10^{-3}$ Torr almost instantaneously.

A typical interruption under vacuum conditions is illustrated in Figs. 21(a) and 21(b). The results are summarized in Figs. 22(a) and 22(b).

TABLE IV: ENERGY TRANSFER PARAMETERS FOR SSI-2 AND IND-1

	3 atmospheres N ₂					1 atmosphere air					1 micron air					10 ⁻⁴ mm air									
	.061	.160	.236	.500	.500	.061	.160	.236	.500	.500	.061	.160	.236	.500	.500	.061	.160	.236	.500	.500	.061	.160	.236	.500	
Load Resistance (ohm)																									
% of Total Energy in Perfect Transfer	32	55	65	80		32	55	65	80		32	55	65	80		32	55	65	80		32	55	65	80	
Energy Transferred (joules)	--	164.5	185	198.4		104	115	137.	170		112.5	122	96	69		112	128	99	70		112	128	99	70	
% of Total Energy	--	44.5	50	54		28	31	37	46		30.5	33	26	19		30	35	27	19		30	35	27	19	
% of Perfect Transfer	--	81	77	67		87.5	56.4	57	57.6		95	60	40	23.4		94.6	63	41	23.6		94.6	63	41	23.6	
Maximum Voltage Across the Load (volts)	--	74	105	148		45	65	100	170		50	50	50	50		50	65	60	50		50	65	60	50	
Arc Duration (msec)	--	<.2	.4	2.4		<.1	.4	1.2	2		<.1	4	8	10		<.1	3.8	8	10		<.1	3.8	8	10	

VIII) MAGNETICALLY ACTIVATED FLUID-METAL INTERRUPTERS

1) Theoretical Considerations

a) Magnet-Driven Interruption

The solid element interrupter configuration is limited regarding repetition rate. A new geometry which obviates this restriction makes use of the same basic geometry as in the single-shot interrupter: a strong pulsed magnetic field is used to displace a DC contactor, and at the same time prevents sparking across the contactor. The problem is that the contactor must be of small size, and will therefore tend to create a heat-removal problem when high repetition rates are used. The natural solution is to employ a conducting fluid in the role of DC contactor (see Fig. 23). The mass of fluid that has to be displaced then still remains moderately small, and the heat is carried off readily by the bulk of the fluid. Another advantage is that an ordinary contactor would tend to erode, whereas the fluid presents no such problem. The principal remaining problems are the cooling of the pulsed magnet that displaces the contacting fluid, and the minimization of erosion at the contact electrode.

To find the opening time of the contact, we imagine a fluid flow-pattern like that in Fig. 24. If the width of the depression in the fluid is \underline{a} , and the depth of the depression is \underline{d} , then for incompressible flow in a layer of thickness s we have

$$\nabla \cdot \mathbf{V} = 0 \quad (1)$$

$$V_x/a = V_z/s \quad (2)$$

and the kinetic energy per unit surface area is

$$\frac{s}{2} \rho \cdot (V_x^2 + V_z^2) = \frac{1}{2} \rho V_z^2 \left(s + \frac{a^2}{s} \right) \quad (3)$$

This is minimized for $s = a$, and we have then for an opening time τ ,

$$d \frac{B^2}{8\pi} = \rho \frac{d^2}{\tau^2} a \quad (4)$$

where we have equated magnetic work and kinetic energy per unit area.

Thus

$$\tau = \sqrt{\frac{8\pi\rho a d}{B}} \quad (5)$$

The characteristic opening time is the transit time at Alfvén velocity over the geometric mean of \underline{d} and \underline{a} .

The best results would be achieved with liquid sodium under a layer of light oil. In that case, for $B = 20$ kilogauss and $a = 1$ cm, $d = .2$ cm, one would obtain $\tau = 100$ μ sec. Thus, a rather weak pulsed field is sufficient.

The technique of heating sodium under oil is very straight-forward, and as soon as a high repetition rate is reached, one can switch to cooling the sodium instead of heating it. For a preliminary experiment one could use mercury, but this has the disadvantages of much greater mass density ρ , and poorer electrical contact and conductivity. The latter feature is important, particularly to insure good coupling to the interrupter magnet. The skin depth

in liquid sodium is about

$$\delta = 30 \tau^{1/2} \quad (6)$$

which gives $\delta = .3$ cm in the above example of $\tau = 100$ μ sec, while mercury would give the much less satisfactory figure of $\delta = 1$ cm, as well as tending to give slower τ .

b) Self-Field Driven Interruption

The magnetic pressure due to the current that is being interrupted will tend to make a crater in the liquid metal (see Fig. 25). This effect could become appreciable for currents on the order of kA and higher. As a matter of fact, this effect could be used for current interruption by itself, without an auxiliary coil (Self-Field-Driven Interruption Mode).

The way to calculate the effect is

$$|j \times B| \approx |\rho g| \quad (7)$$

If the inductance current is turned on rapidly, so that there is skin effect, then Eq. (7) means roughly

$$B^2/8\pi = I^2/(25 \cdot r^2 \cdot 8\pi) = h\rho g \quad (8)$$

where I is the current in amps and h is the depth of the resultant depression.

For $I = 1000$ amps, and liquid sodium, we have roughly

$$hr^2 = 1.5 \text{ cm}^3 \quad (9)$$

This indicates that the radius of the contactor should not be too small. For mercury this effect is less important. It might be expedient to make a contactor where the pulsed interrupter field can get through (see Fig. 26a). If the inductance current is turned on slowly, the situation is less critical because the magnetic field penetrates into the liquid metal (see Fig. 26 b). That means the magnetic pressure term is less effective, and we have

$$|\mathbf{j} \times \mathbf{B}| \sim B^2 / 8\pi R \quad (10)$$

where R is the thickness of the current layer. Then R takes the place of h in Eq. (8), and no such deep depressions result.

In order to handle high storage currents, the contact perimeter has to be made large. For example, we might consider the geometry outlined in Fig. 27(a) which, upon pulsing of the coil, generates the situation illustrated in Fig. 27(b), where the arcs would race around in a circle, producing a back-voltage. The strength of the interrupter field would control the back-voltage perfectly. Therefore, this is a kind of power amplifier.

For the case when the storage current is turned on slowly, the configuration in Fig. 28 does not produce a depression at all, even at strong currents. The reason is that, because of the up-down symmetry, the $\mathbf{j} \times \mathbf{B}$ pressure is purely radial. There is, of course, the possibility of setting up MHD turbulence in the liquid metal, thus increasing the resistance.

Another possibility is to use the pinch effect to advantage in getting the desired back-voltage, as outlined in Fig. 29.

If the interrupter capacitor is fired, a back-voltage is immediately established against the storage inductance (i.e., across the load), and the current flowing through the liquid-metal interrupter can be greatly increased. As a result, the electrode loses contact, and a pinch develops in the liquid element. The capacitor serves to regulate the voltage by acting as a reservoir.

c) Stability of the DC Contact

For strong DC currents the column of metal making the DC contact will become unstable, thus leading to premature current-interruption. There are two basic types of instability: the "sausage" mode, which is axisymmetric, and the "kink" mode, which is the lowest-order asymmetric mode. New liquid metal, of course, tends to move in where the old is displaced, but turbulence and arcing will easily result (see Fig. 30).

The stability condition against the sausage mode is ⁵

$$-r (dp/dr) < 2\gamma p B_{\theta}^2 / (B_{\theta}^2 + 4\pi\gamma p) \quad (11)$$

where p is the fluid pressure, γ is the ratio of specific heats, in our case very large, and B_{θ} is the azimuthal field of the DC current, which is related to p by the pressure-balance condition

$$(dp/dr) + \frac{1}{4\pi} \frac{B_{\theta}}{r} \frac{d}{dr} (r B_{\theta}) = 0 \quad (12)$$

In the region of current flow, we have roughly uniform current density i_z in the DC limit, so that from

$$4\pi i_z = \frac{1}{r} \frac{d}{dr} (r B_\theta) \quad (13)$$

we get

$$B_\theta \sim r \quad (14)$$

Now from Eq. 11 we have, for large γ

$$-(dp/dr) < B_\theta^2 / 2\pi r \quad (15)$$

and using Eq. 12, we get

$$d(r B_\theta) / dr < 2 B_\theta \quad (16)$$

Thus we see that $B_\theta \sim r$ is just marginally unstable. If i_z gets weaker at large radii (which, in fact, it will do in practice), then B_θ will rise less strongly than r , and Eq. 16 will predict stability against the sausage mode. If, on the other hand, the current is pulsed on rapidly, then skin effect may cause B_θ to increase radially more rapidly than r , and the sausage mode may occur.

The condition against the kink mode is⁵

$$r (dB_\theta / dr) < -\frac{1}{2} B_\theta \quad (17)$$

which is impossible to satisfy in the region of the current flow. Hence, the kink mode is always unstable. This mode, however, is a little less vicious than the sausage; furthermore, in a short column of fluid, allowing for finite fluid viscosity and surface tension, it may be effectively stabilized. If not, there may be some point in adding a weak DC B_z -field, as from a permanent magnet.

2) Studies with Liquid Mercury Interrupter Configuration MSI-1

The first fluid metal interrupter developed made use of liquid mercury and is illustrated schematically in Fig. 31. The electrode height adjustment nut allows accurate positioning of the electrode with respect to the mercury surface. Windows are for observation during the testing phase.

In operation, the opening times of the switch will depend on three parameters: (i) height of the coil above the fluid; (ii) depth of electrode in the fluid; (iii) energy at which the coil is fired.

Height of the coil above the mercury is adjustable only by varying the amount of mercury in the switch. Depth of the electrode is continuously adjustable even under high vacuum or a pressurized atmosphere.

The MSI-1 coil consists of two kidney-shaped coils connected in parallel, one wound clockwise, the other counterclockwise, as shown in Fig. 32(a). Each coil consists of 9 turns of $1/2'' \times 1/32''$ copper strip and the inductance of the configuration after being potted in epoxy is $2.4 \mu\text{h}$, the resistance about 0.1Ω with the

coils in parallel. This configuration has been tested successfully to energies up to 935 joules ($29 \mu\text{f} - 8 \text{ kv}$) and hence to currents on the order of 28 kiloamps. Fields thus produced are on the order of 30 kilogauss without a load, and on the order of 40 kilogauss with a soft iron plate above the coil surface. These fields are considered sufficient for producing displacements in the mercury fluid metal type interrupter switch. Deformation of 1.5 mil aluminum foil, placed over the coil face was studied to simulate the stress distribution on the liquid metal surface. Deformations of elliptical cross section (see Fig. 32 b) ($a = 4 \text{ cm}$, $b = 3 \text{ cm}$) and depth = .5 cm were produced at the planned electrode location. At higher energies, above 360 joules, the aluminum foil was ripped apart by the magnetic forces.⁶ The magnetic field profiles of the H_z and H_r components are given in Fig. 33(a) and 33(b).

Tests to determine the opening times of the MSI-1 have proceeded as follows: a six volt battery with a current limiting resistor was placed across the MSI-1 terminals. Oscillograms were taken of the voltage drop across the terminals as the interrupter coil was fired at various voltages.

Very fast opening times were observed: 24 μsec , 30 μsec and 34 μsec for energizing coil voltages of 9 kv, 7 kv and 5 kv, respectively. An oscillogram of the 9 kv shot is included as Fig. 34. These opening times were observed before the MSI-1 was incorporated into the IND-1 circuitry; the electrode (stainless steel) was clean and unscarred. However, after passage and interruption of high currents

(~ 600 amps) the electrode became pitted and the mercury wetted the electrode tip. Under these conditions, the mercury surface had to be depressed until the weight of the mercury column under the electrode became sufficient to overcome the surface tension of the mercury and opening could occur.

Low inductance loads (made of .005" stainless steel strips about 0.5" wide and folded) of .200 Ω , .420 Ω , and .733 Ω were used in the high current interruption mode. The measured inductance of the .733 Ω load was < 3 μ h, for all other loads $L \approx 100$ nh or less.

We have found that using very small loads reasonable energy transfer could be achieved by self-interruption, i.e., using the current's own field to move the fluid-metal away from the electrode. In one instance, with a .074 Ω load, self-interruption was able to produce a transfer that was 72% of perfect.

Experiments were performed with the IND-1 energized to 370 joules and with the MSI-1 operated at different pressures. As in the case with the SSI-2, the best transfer efficiencies were achieved under pressurization. Table IV summarizes the results obtained using the MSI-1 liquid-metal interrupter in the magnet-driven mode. Figures 35(a) and 35(b) are graphs of the same data.

TABLE V: ENERGY TRANSFER PARAMETERS FOR MSI-1
AND IND-1

(Magnet-Driven Mode)

	2 atm N ₂			4 atm N ₂			6 atm N ₂		
Load Resistance (ohm)	.200	.420	.733	.200	.420	.733	.200	.420	.733
% of Total Energy in Perfect Transfer	60.6	76.4	84.2	60.6	76.4	84.9	60.6	76.4	84.9
Energy Transferred (joules)	64.25	33.1	28.7	45.5	49.9	27.3	75.4	62.5	33.1
% of Perfect Transfer	28.8	11.72	9.11	20.3	17.67	8.67	33.7	22.1	10.54
% of Total Energy	17.5	8.95	7.71	12.3	13.5	7.37	20.4	16.9	8.95
Maximum Voltage Across the Load (volts)	47.2	50	62	42.2	64.8	58.5	39.0	67.6	66.9
	Atmospheric			~ 10 μ of Hg					
Load Resistance (Ω)	.200	.420	.733	.200	.420	.733			
% of Total Energy in Perfect Transfer	60.6	76.4	84.9	60.6	76.4	84.9			
Energy Transferred (joules)	41.2	21.2	20.8	---	<1	2.2			
% of Perfect Transfer	18.3	7.6	6.6	---	<.36	.7			
% of Total Energy	11.1	5.7	5.6	---	<.28	.6			
Maximum Voltage Across the Load (volts)	35.1	45	47.3	---	5	14			

3) Studies with Liquid Sodium Interrupter Configuration MSI-2

A second liquid metal interrupter was developed in which use was made of a molten sodium pool. The MSI-2 interrupter switch has been incorporated into the IND-1 circuitry previously described. As before, an ignitron crowbar was employed to remove the charging capacitors from the inductance-load-MSI-2 circuit when the current in the IND-1 has reached maximum.

First, the self-interruption process was investigated. The merits of such system are many: it obviates the need of a power supply, trigger unit and driving coil, and, theoretically, could give a higher repetition rate than an externally-driven system. The biggest single problem thus far encountered is that of not interrupting until several milliseconds after the current has reached maximum (see data in Table VI). The delay is due to scarring of the contact electrode and surface impurities in the sodium. The scarring is a result of arcing and can be reduced by making the arc path more resistive (higher pressure) and, consequently, transferring more of the IND-1 energy to the load and less to the arc.

Results from the analysis of data taken with a $.074 \Omega$ load is displayed as Table VI. As noted in the table, both energy-transferred and %-of-perfect-transfer climb rapidly as the pressure is increased. Reading down a column at constant pressure shows that although the energy-transferred increases, the %-of-perfect-transfer decreases as the energy in the IND-1 is increased. Comparison at constant pressure and energy for more resistive loads shows, with few exceptions, both less energy-transferred and a smaller %-of-perfect transfer.

Results from the MSI-2 in the magnet-driven mode are incomplete but the data available is very promising indeed.

Using the driver coil powered from a 22 μ f capacitor bank at 3 kv, the following has been noted:

At 1 atmosphere pressure and with the IND-1 energized to 360 joules upon interruption 88 joules were transferred to the .074 Ω load. This is 22.5% of the total stored energy and 62% of a perfect transfer with a stand-off voltage of 22 volts.

At 2 atmospheres and same IND-1 energy, 113 joules was transferred to the load, 29% of the stored energy and 79.7% of a perfect transfer with a stand-off voltage of 30 volts.

Comparing these to Table VI (columns 1 and 2, top row), it is seen that by using the externally driven mode, increases of 21% and 27% were achieved in the %-of-perfect-transfer column.

At 5 atmospheres, with the IND-1 energized to 1440 joules, 400 joules were transferred to the load. This transferred 28% of the stored energy with a "perfect transfer" percentage of 78% and a stand-off voltage of 65 volts. With a stand-off voltage (maximum voltage applied to the switch without arcing) of 65 volts, we are able to produce perfect transfers into loads of up to 130 m Ω when the IND-1 is energized to 360 joules, up to 87 m Ω with the IND-1 at 810 joules and up to 65 m Ω with the IND-1 at 1440 joules (see Fig. 36).

These shots all show significant increases over those conducted in the self-interrupting mode and the trend is expected to continue over the entire range.

As a note on the wide discrepancy in the % of perfect transfer and % of total energy in Table VI, the load plus the circuit resistance totals $\sim 20 \text{ m}\Omega$, showing that the best transfer possible is 36% for the $.074 \Omega$ load. We would, however, expect the %-of-perfect-transfer to remain constant as the IND-1 was lowered to LN temperatures. This should cut the circuit resistance to $\sim 20 \text{ m}\Omega$ and consequently make the perfect transfer $\sim 79\%$ of the total IND-1 energy. Then with 80% of perfect transfer we will transfer $\sim 65\%$ of the total stored energy.

TABLE VI

SYNOPTIC TABLE OF ENERGY TRANSFER PARAMETERS WITH MSI-2 AND IND-1
(Self-Field-Driven Mode)

.074 Ohm Load

(Pressurization with Dry N₂)

IND-1 Energy	1 Atmosphere	2 Atmospheres	3 Atmospheres	4 Atmospheres	5 Atmospheres	Energy Transferred % Total Energy % Perfect Transfer
360 joules 800 μf-1 kv	53.5 joules 14.8% 41%	68.5 joules 19.0% 52.3%	60.9 joules* 16.9%* 46.4%*	72 joules* 20%* 55%*		
810 joules 800 μf-1.5 kv	94.6 joules 11.6% 31.9%	72.1 joules* 8.9%* 24.5%*	147.5 joules 18.2% 50%	132 joules 16.2% 44.6%*	87.1 joules* 10.8%* 30%*	Energy Transferred % Total Energy % Perfect Transfer
1440 joules 800 μf-2 kv	113 joules 7.8% 21.5%	160.9 joules 11.2% 30.7%	168 joules 11.6% 31.9%	210 joules 14% 38.5%	300 joules 20.8% 57%	Energy Transferred % Total Energy % Perfect Transfer

* Interruption did not take place until well after current maximum.

IX) CONCLUSIONS

The initial experiments with liquid-metal interrupters have demonstrated all the expected features. The predicted self-interruption phenomenon has been observed, and in itself gives moderately efficient energy transfer. Again as expected, however, the use of an auxiliary coil for interruption is more effective. Mercury was adequate to demonstrate the principles of the switch, but liquid sodium shows a dramatic improvement, as calculated on the basis of its lower mass density and higher conductivity ($\rho_{\text{Hg}} = 13.55 \text{ gm/cm}^3$, $\rho_{\text{Na}} = 0.93 \text{ gm/cm}^3$; $\eta_{\text{Hg}} = 98.5 \mu\Omega \cdot \text{cm}$, $\eta_{\text{Na}} = 9.8 \mu\Omega \cdot \text{cm}$).

Fairly satisfactory operation is achieved already in the present liquid-sodium switch (best transfer, 80% of ideal transfer, 65% of total stored energy). There are several clear avenues, however, that should lead to much better performance yet.

- 1) The interruption voltage that can be achieved (at present about 80 v) depends on the suppression of arcs, following the physical displacement of the sodium away from the electrode. One clearly demonstrated way of raising this voltage is to use high-pressure gas over the sodium. In a suitably constructed switch, much higher pressures than that presently used could be realized. It would also be of interest to try high-pressure gas over a layer of oil over the sodium.

The second possible line of advance is to use a high vacuum over the sodium, in which case everything depends on the design of the magnetic field and the insulators, so as to prevent breakdown. (This problem and the best approach to its solution have already been discussed above.)

- 2) The maximum current that can be interrupted at high repetition rate will be limited in part by the erosion of the conductor electrode. At present we are interrupting currents of 1000 amps, and the cratering effect of arc spots is already apparent. One promising solution may be to use liquid sodium on both sides of the interruption point. The electrode-erosion problem may, however, yield simply to a study of optimal electrode materials -- possibly a porous electrode, wetted with liquid sodium, for example.
- 3) Even without radical changes in the present design, a smaller, simpler, and more functional unit could readily be developed. A cluster of such switches, even if they did not exceed present performance, could serve to deliver very practical amounts of energy from inductive storage units into loads of interest (pulse transformers in klystron circuitry) at finite repetition rates.

The economical and space saving features of inductive storage are impressive: even at the readily attainable field strength of 25,000 gauss, the energy density is

already 2.5 j/cm^3 versus the usual 0.05 j/cm^3 for electrostatic storage (high voltage capacitors), nearly a factor of 50 in favor of the electromagnetic method. The possibility, then, of storing a full megajoule of energy in a compact volume of only 1 m^3 is a convincing indication that inductive storage might become a most promising element in pulsed radar technology.

REFERENCES

- 1) H. C. Early and R. C. Walker, Conference on Extremely High Temperatures, p. 61 (John Wiley and Sons, 1958) and H. P. Furth, Instrumentation for High Energy Physics, p. 1 (Interscience Publishers, 1961).
- 2) O. Anderson, W. R. Baker, A. Bratenahl, H. P. Furth and W. B. Kunkel, J. Appl. Phys. 30, 188 (1959).
- 3) H. C. Early and W. G. Dow, Phys. Rev. 79, 186 (1950).
- 4) K. Halbach, Lawrence Radiation Laboratory, Berkeley, Private communication (1964).
- 5) B. B. Kadomtsev, USSR J. Exp. Theor. Phys. 37, 780 (1960).
- 6) H. P. Furth and R. W. Waniek, Rev. Sci. Instr. 27, 195 (1956) and H. P. Furth, M. A. Levine, R. W. Waniek, Rev. Sci. Instr. 28, 949 (1957).

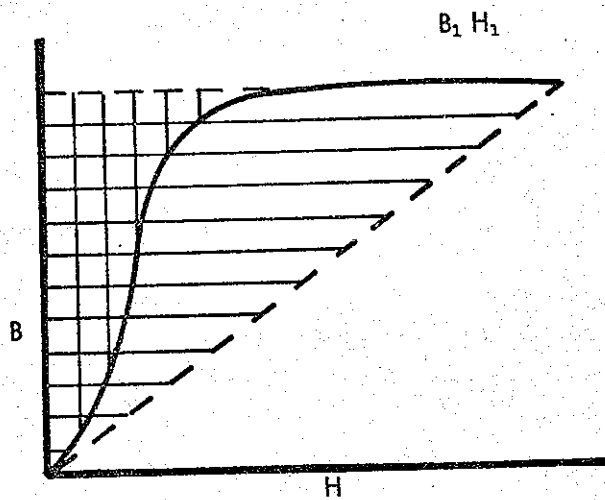


Fig. 1: The \equiv area is $B_1 H_1/2$, while the smaller $\equiv\equiv$ area is $\int_0^{B_1} H dB$. The latter gives a measure of the stored energy density.

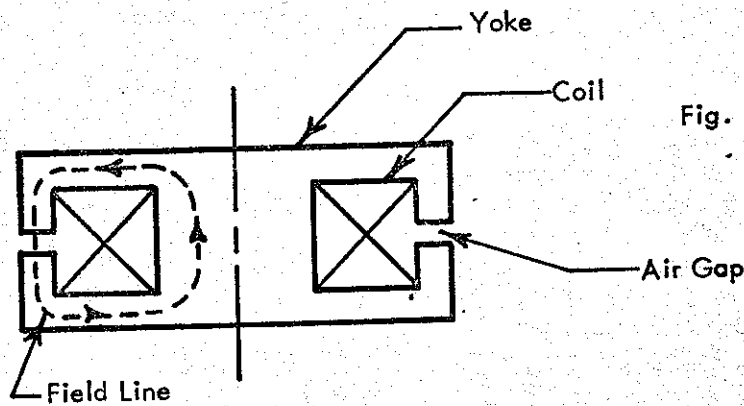


Fig. 2: Inductor with Iron Core

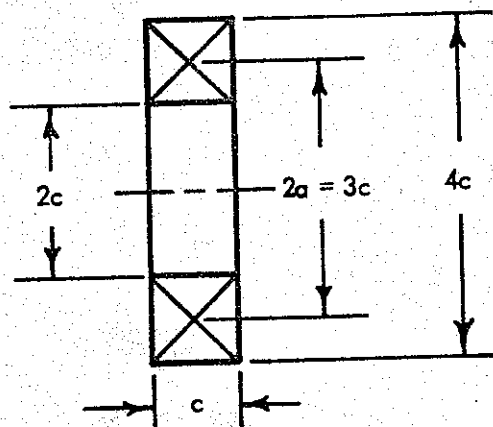


Fig. 3: Brooks Coil

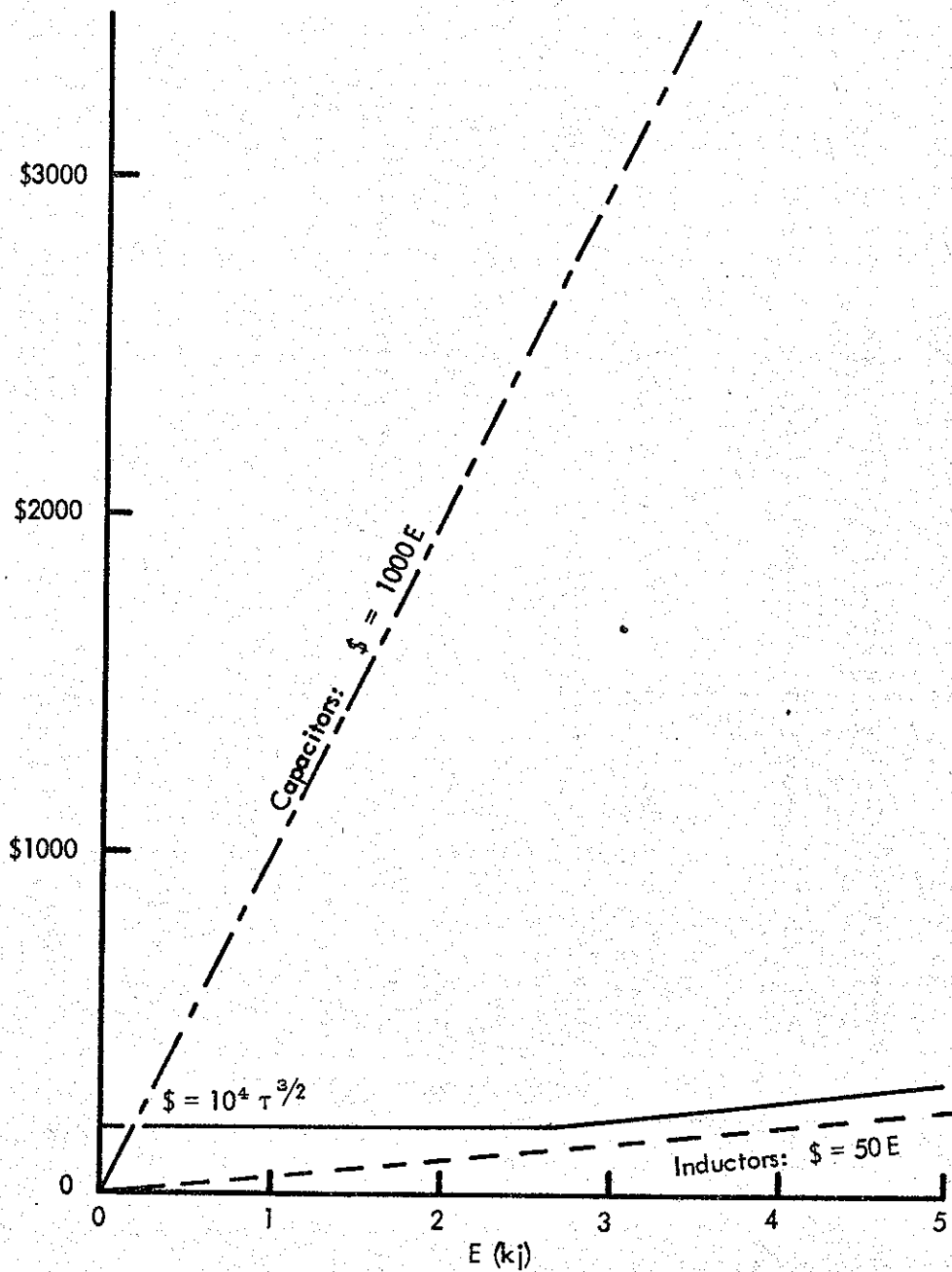


Fig. 4: Projected Costs of Capacitive vs. Inductive Storage

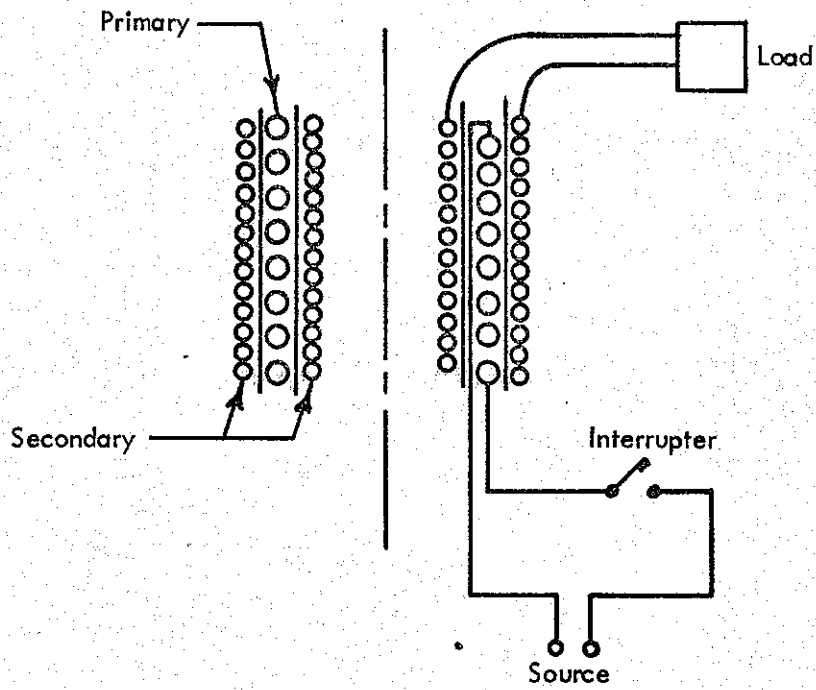


Fig. 5

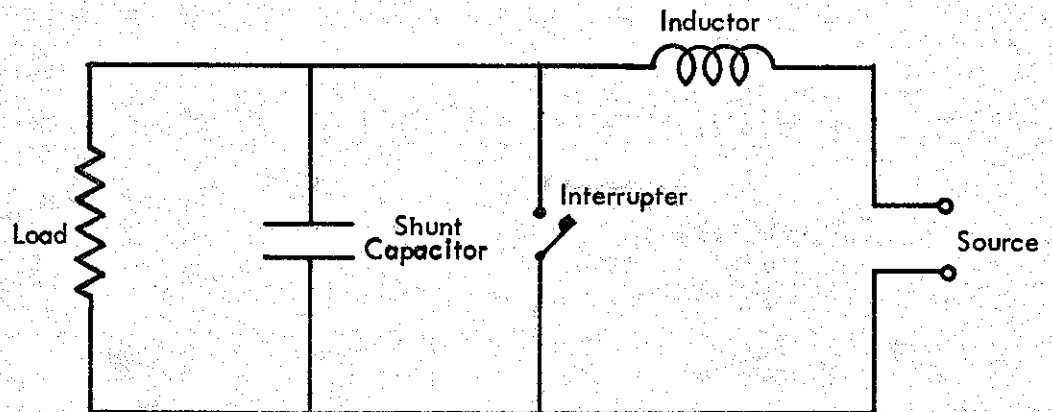


Fig. 6

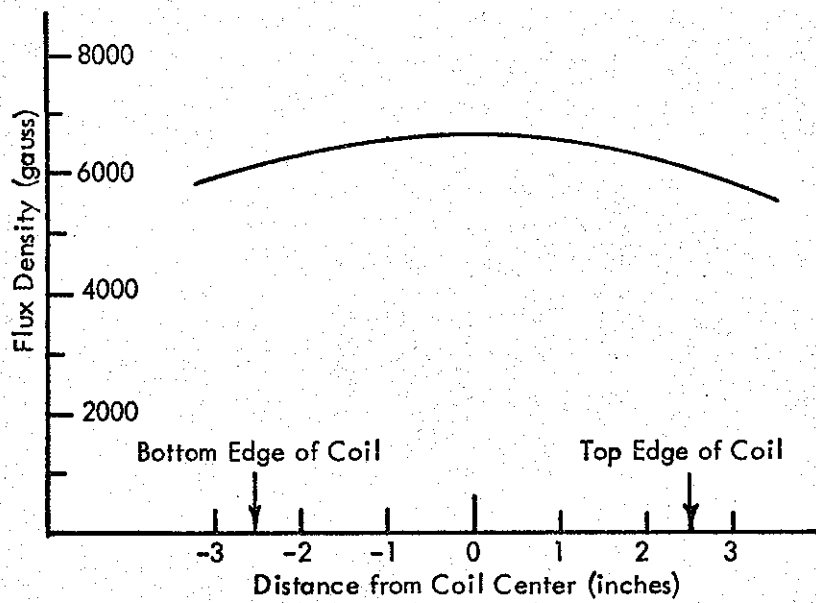


Fig. 7(a): Flux Density Along Axis of IND-1 Storage Coil (6,400 joules)

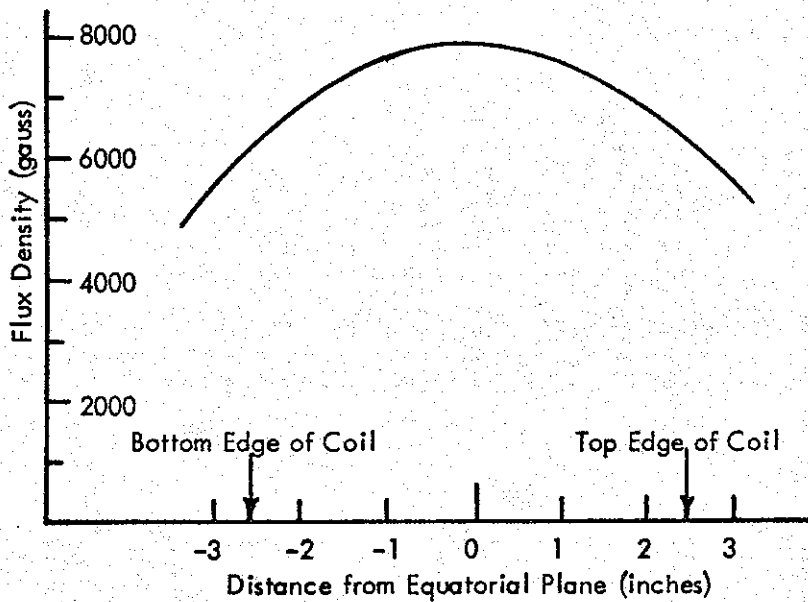


Fig. 7(b): Flux Density Along Inner Wall of IND-1 Storage Coil Parallel to Coil Axis (6,400 joules)

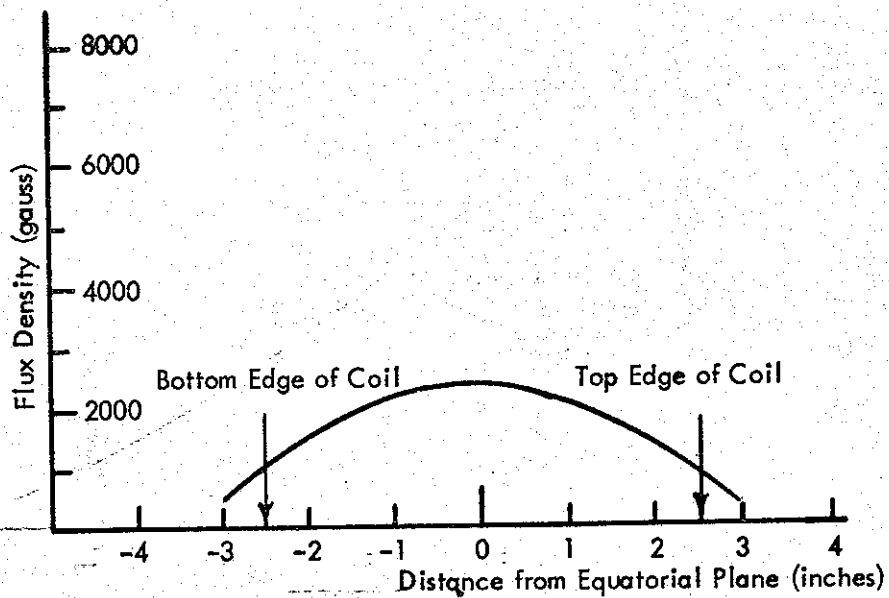


Fig. 7(c): Flux Density Along Outer Wall of IND-1 Storage Coil Parallel to Coil Axis (6,400 joules)

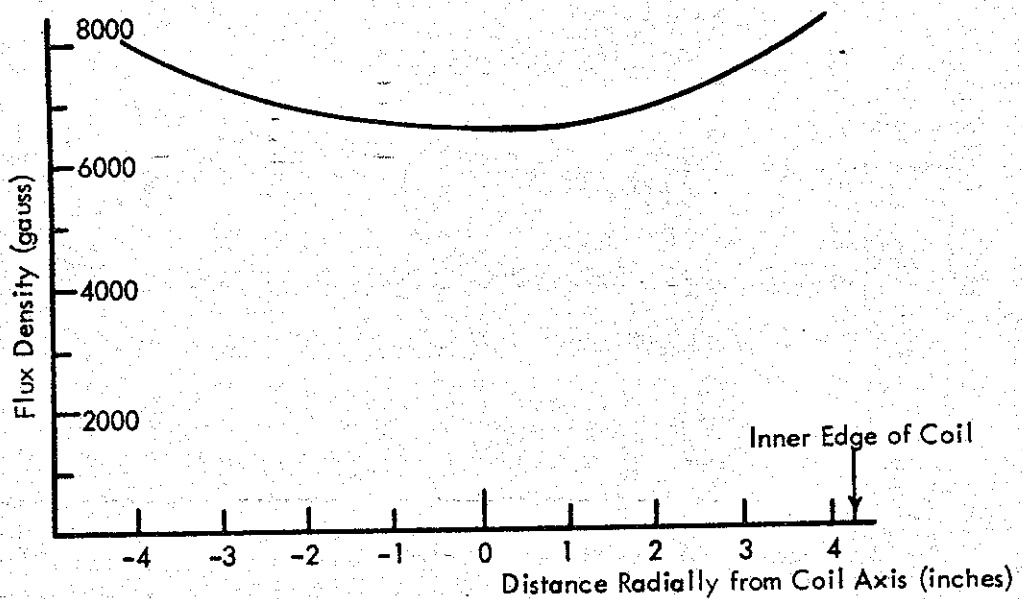


Fig. 7(d): Flux Density of IND-1 Storage Coil in Equatorial Plane (6,400 joules)

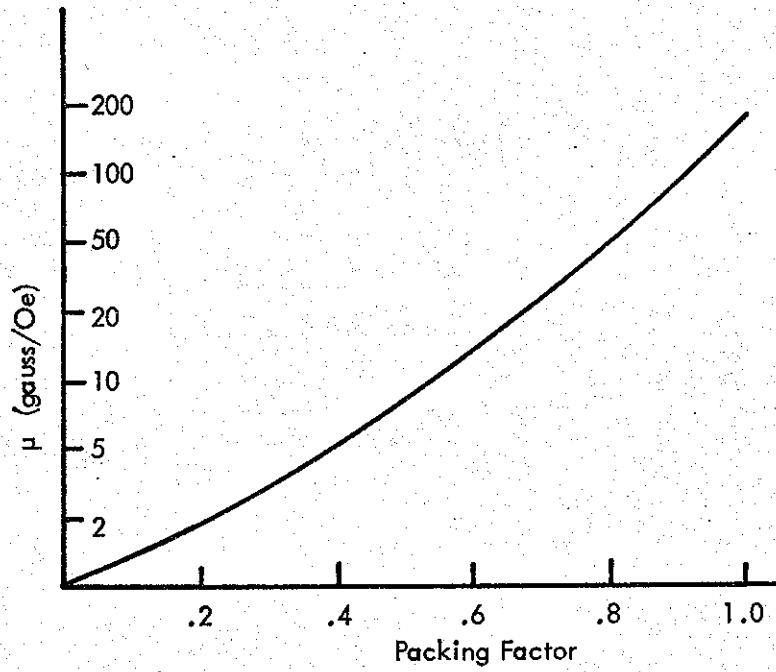


Fig. 8

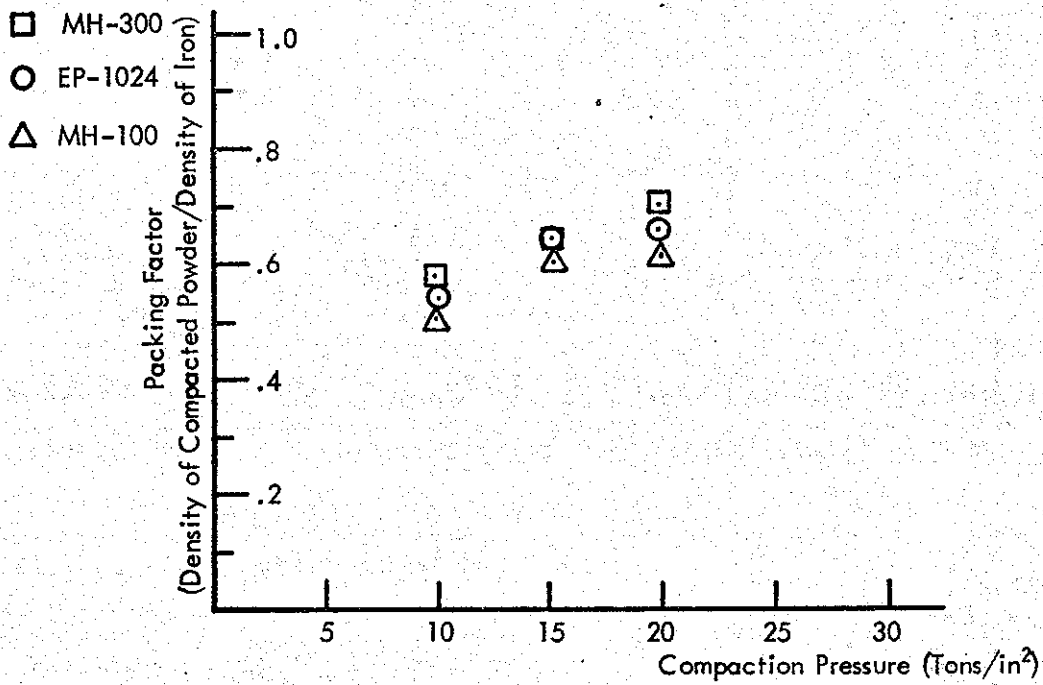
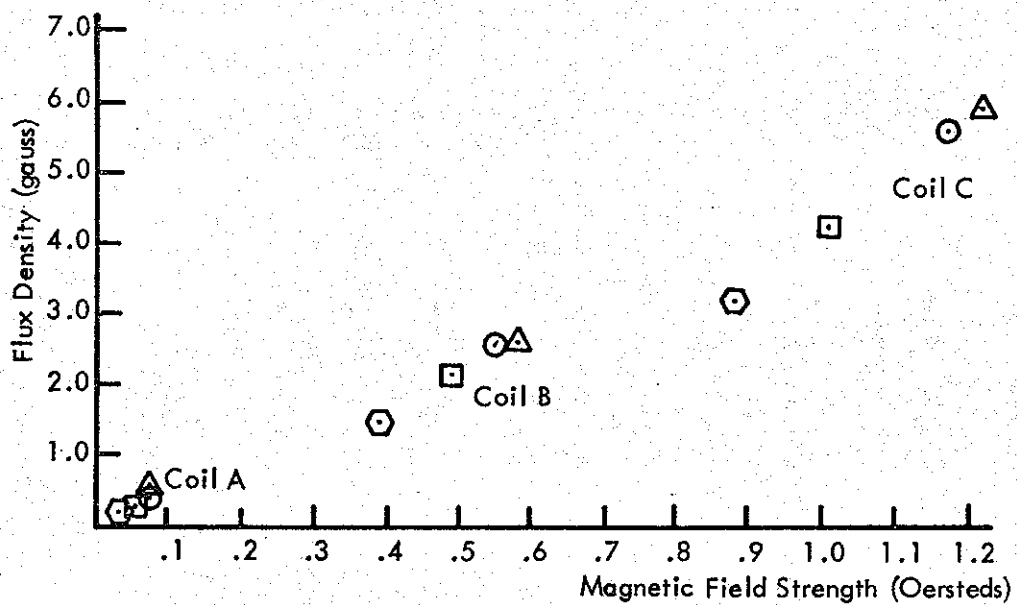


Fig. 10: Powder Packing Factor vs Compaction Pressure



- MH-100 ○
- EP-1024 △
- MH-300 □
- Grade B ⬡

Fig. 9(a): Flux Density vs Magnetic Field Strength
Coils A, B, C

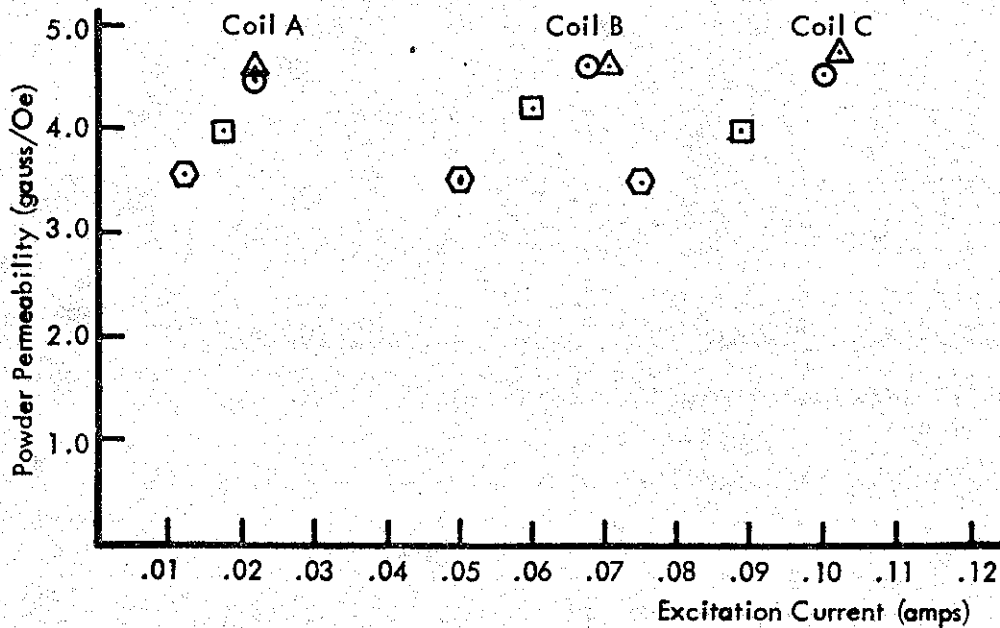


Fig. 9(b): Powder Permeability vs Excitation Current

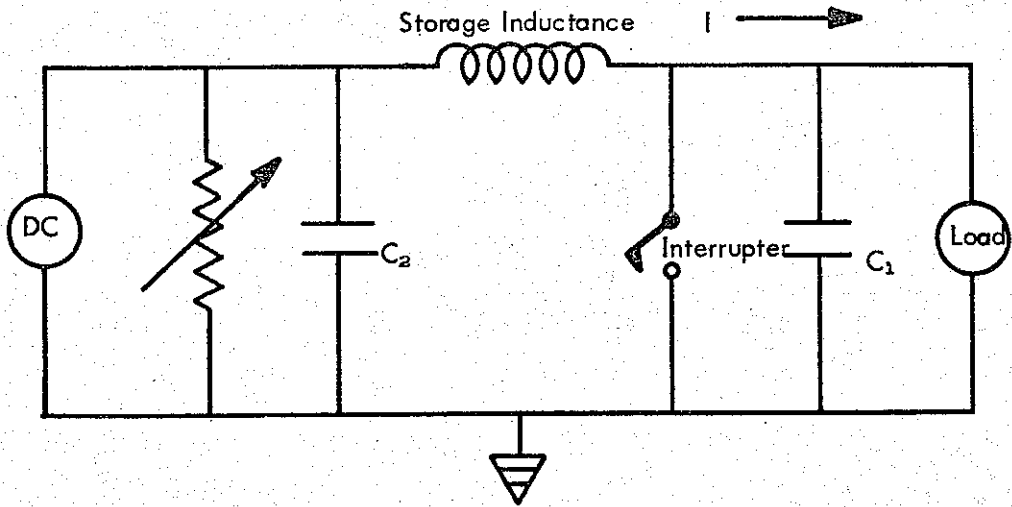


Fig. 11(a)

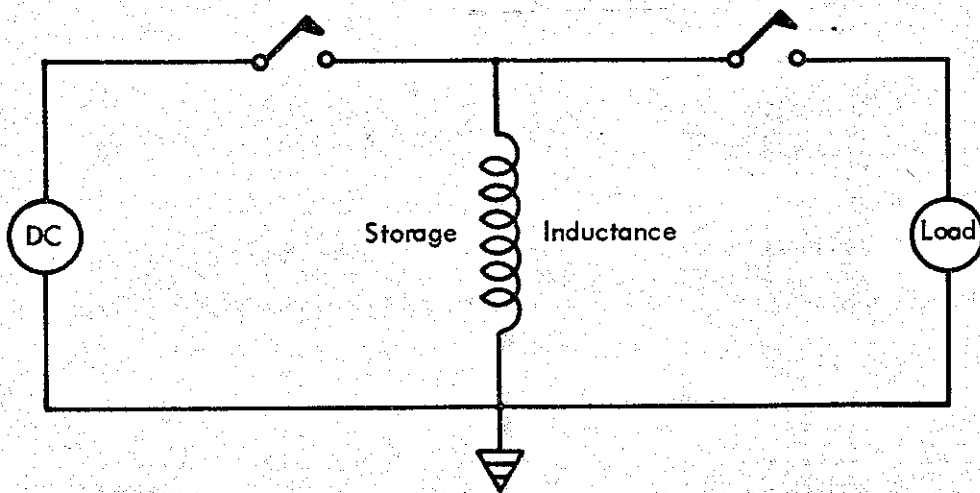


Fig. 11(b)

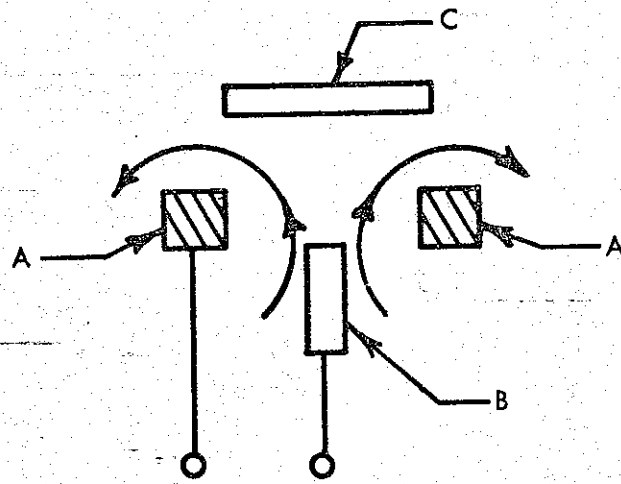


Fig. 12

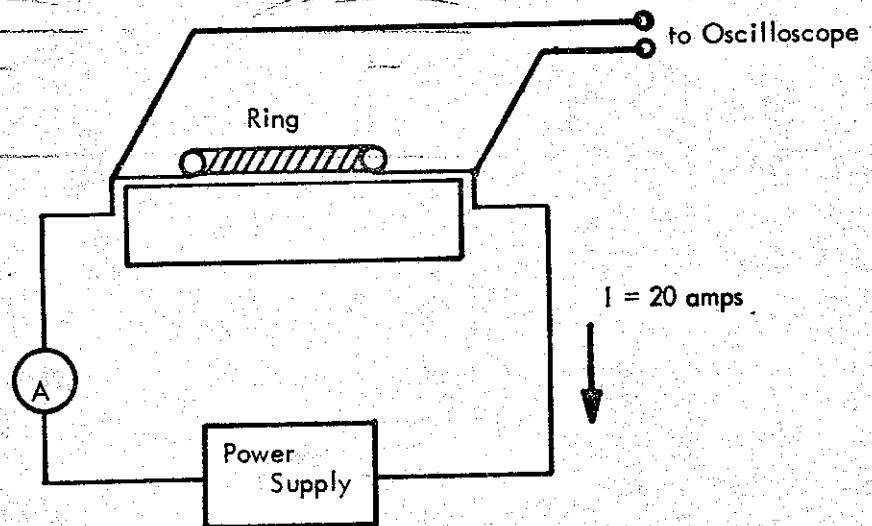


Fig. 14: Test Circuit for SSI Prototype

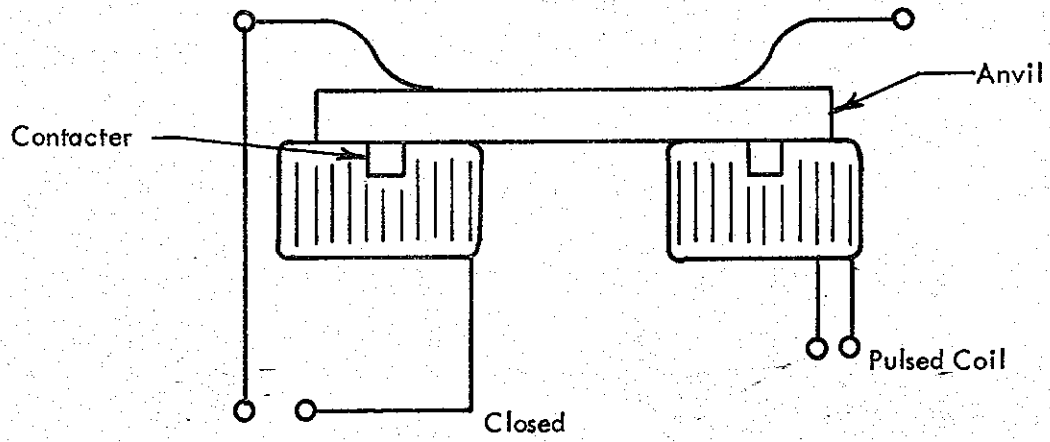


Fig. 13(a)

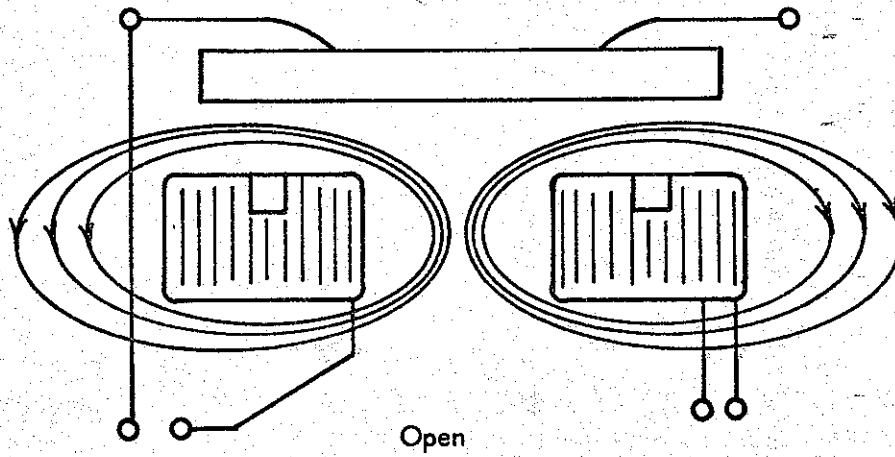
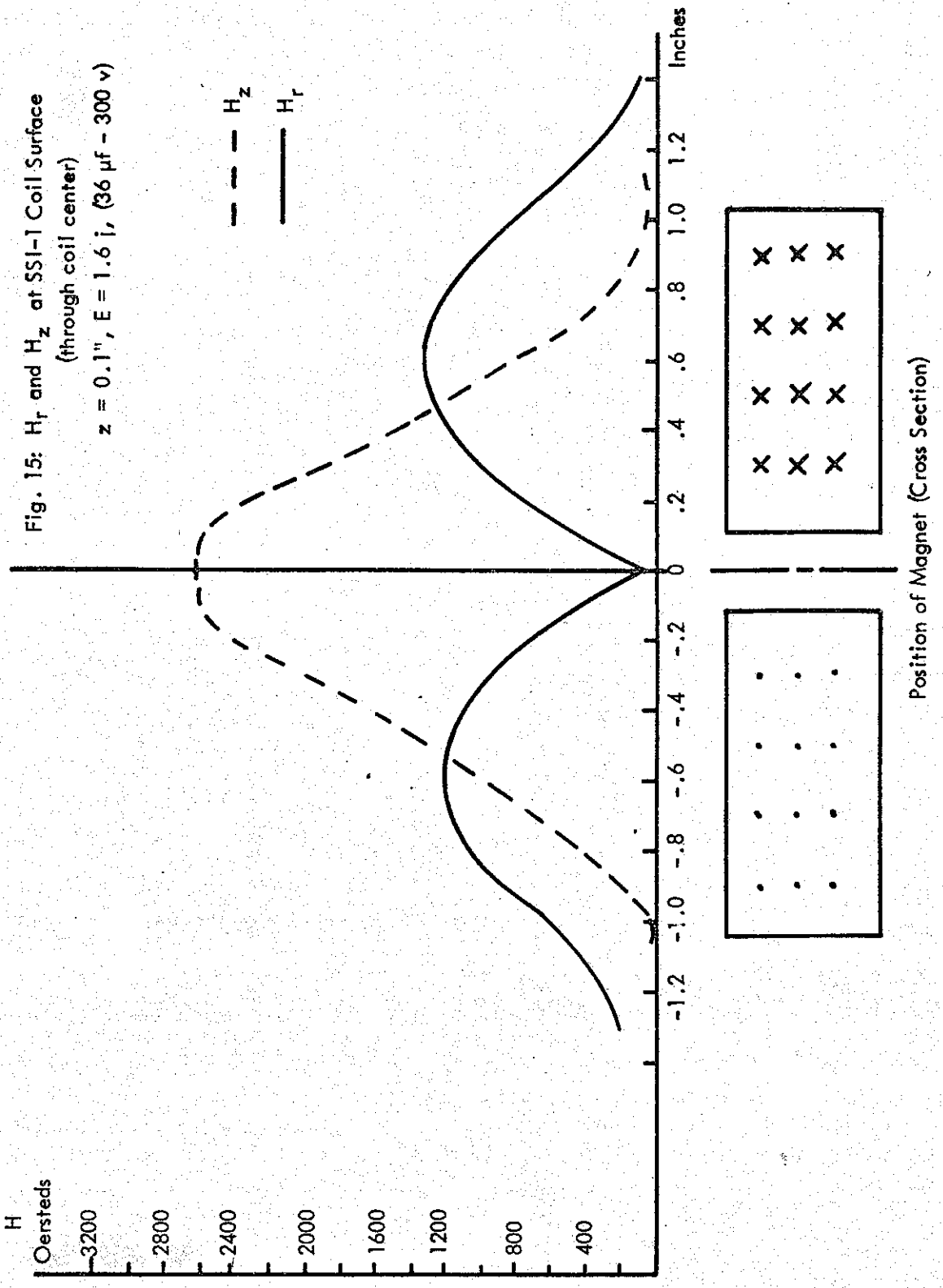


Fig. 13(b)



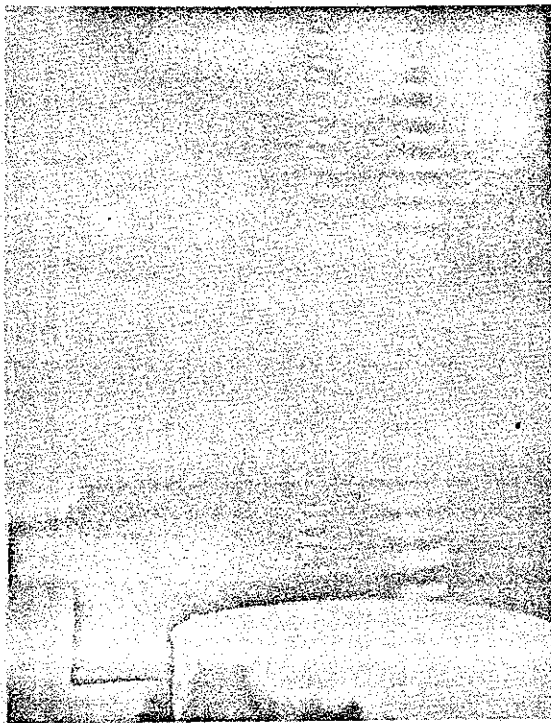


Fig. 16: Stroboscope Photograph

Ring mass 11.1 grams
Energy in driver coil 14.5 joules (1 kv - 29 μ f)
Strobe frequency 400 flashes/sec

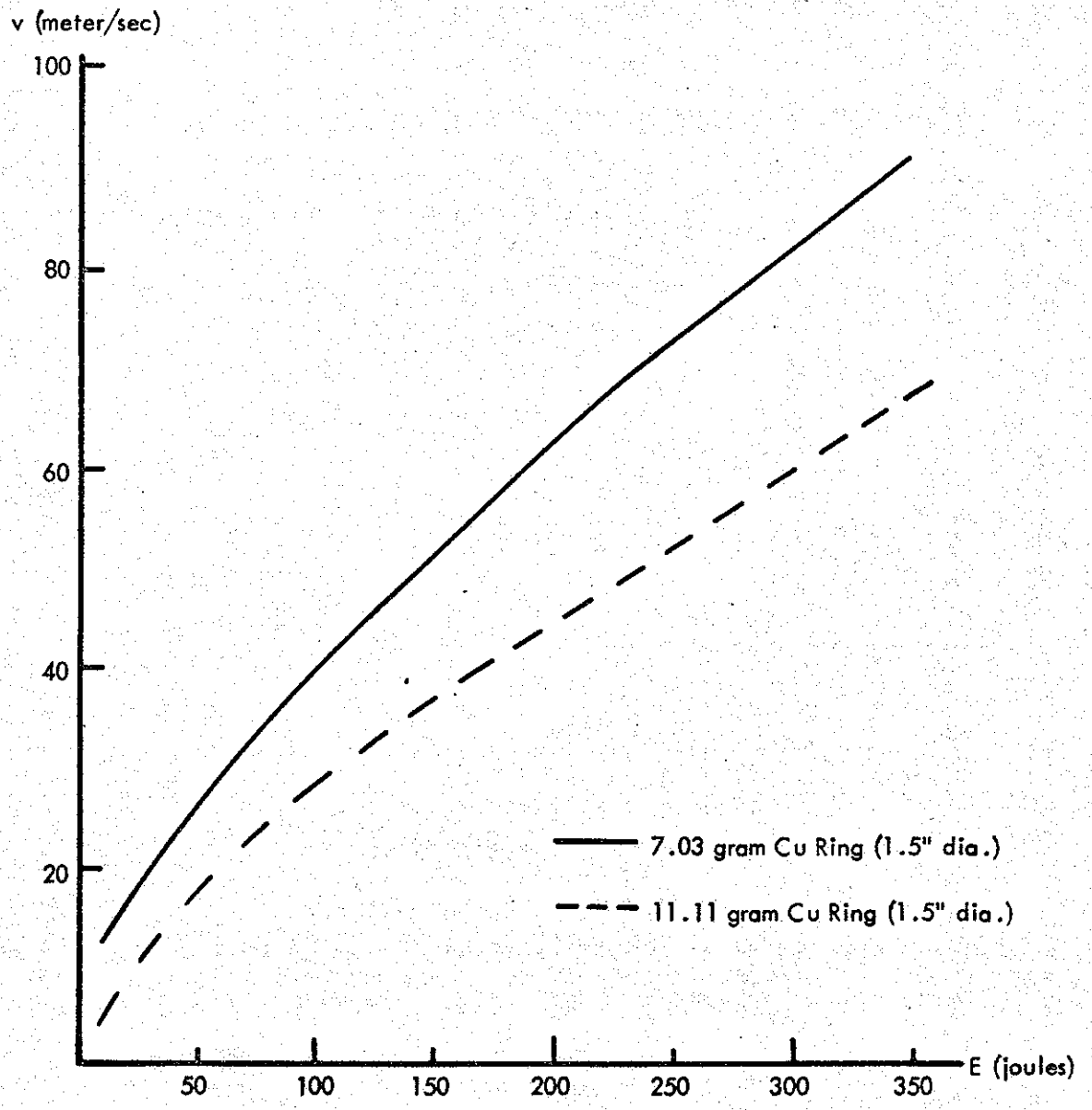


Fig. 17: Ring Velocities vs Firing Energy

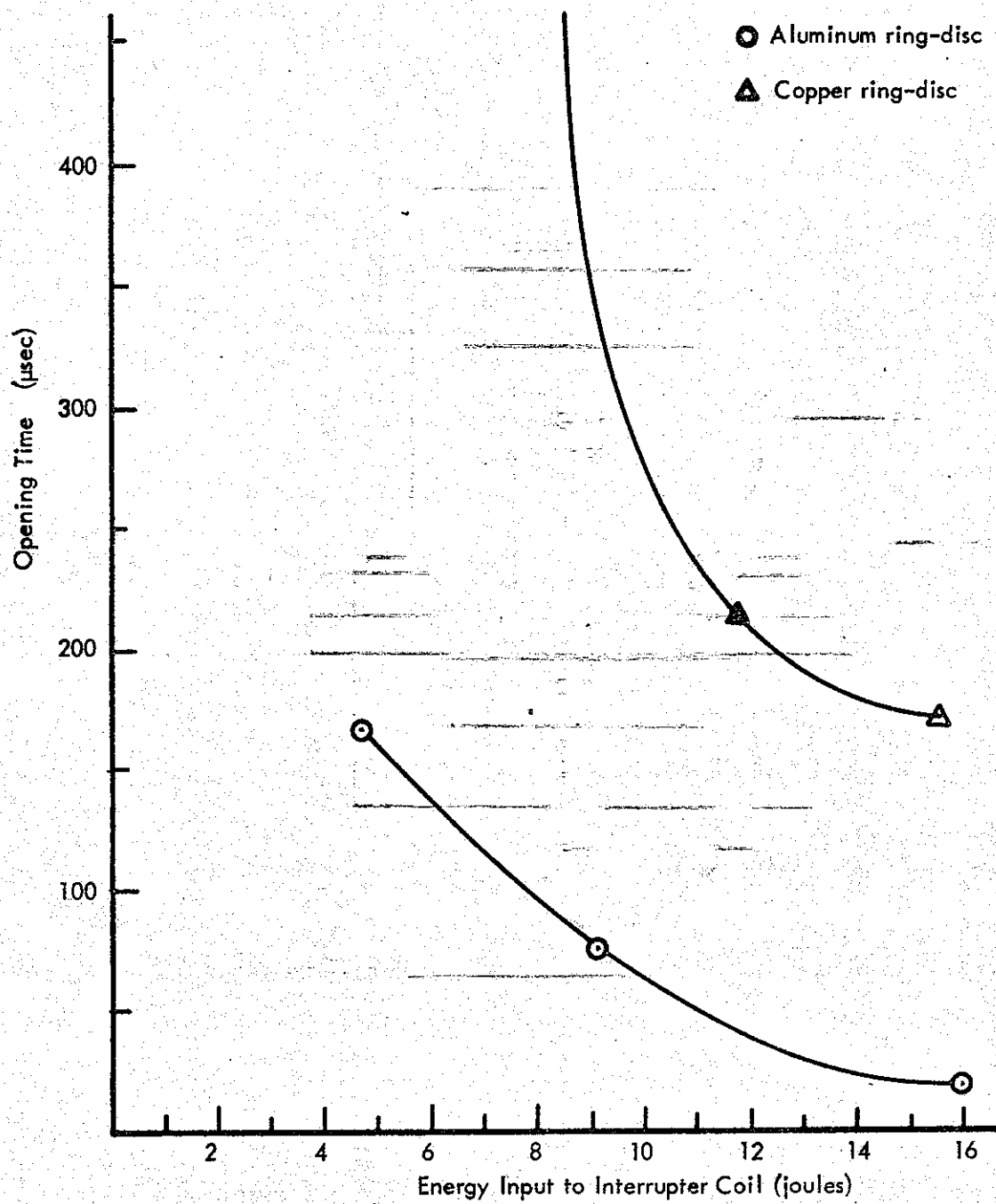


Fig. 18: Interrupter Switch SSI-1 Opening Time vs Energy Input to Interrupter Coil

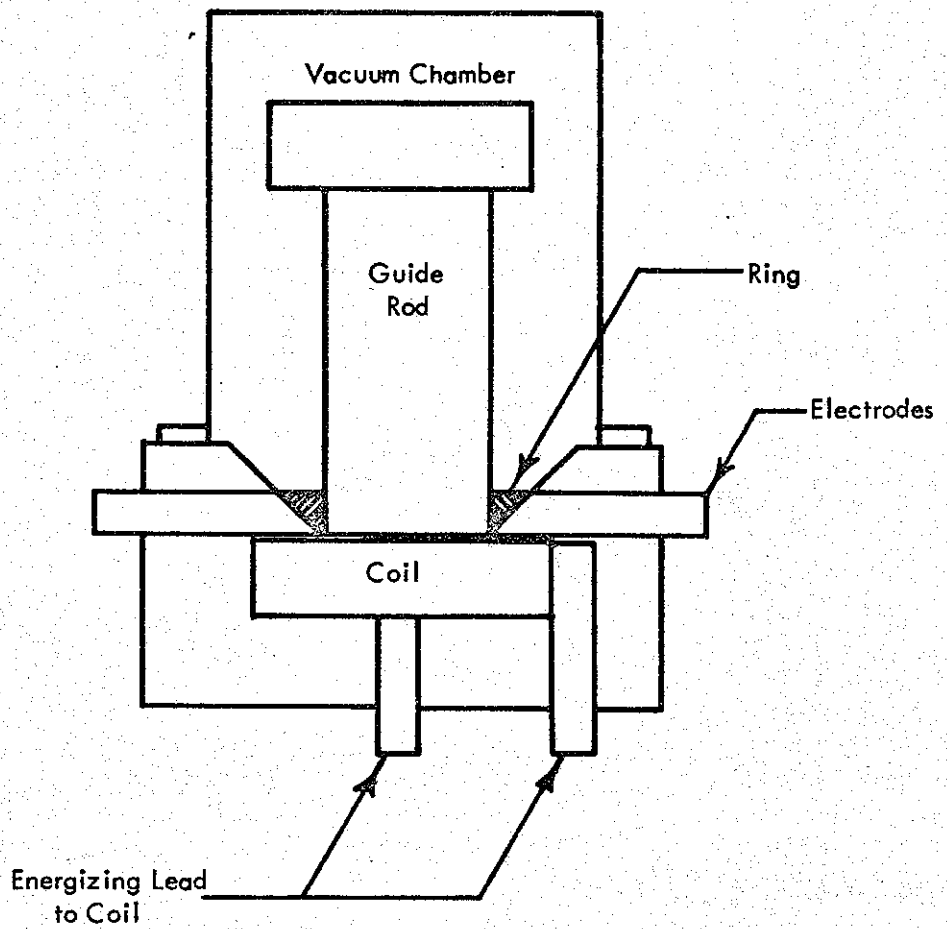


Fig. 19: SS1-2

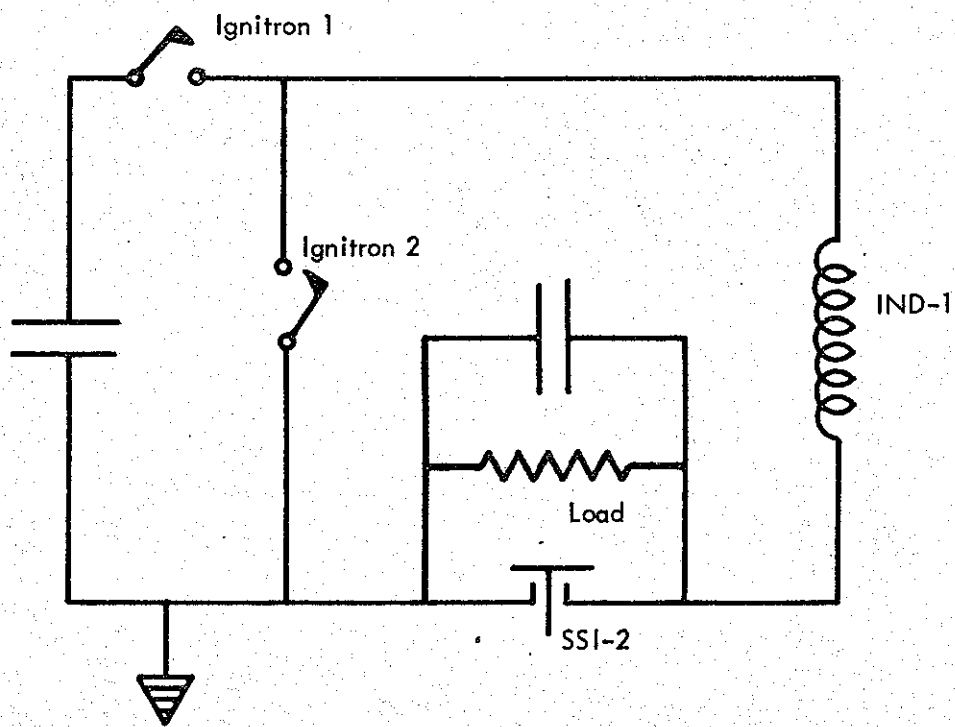


Fig. 20

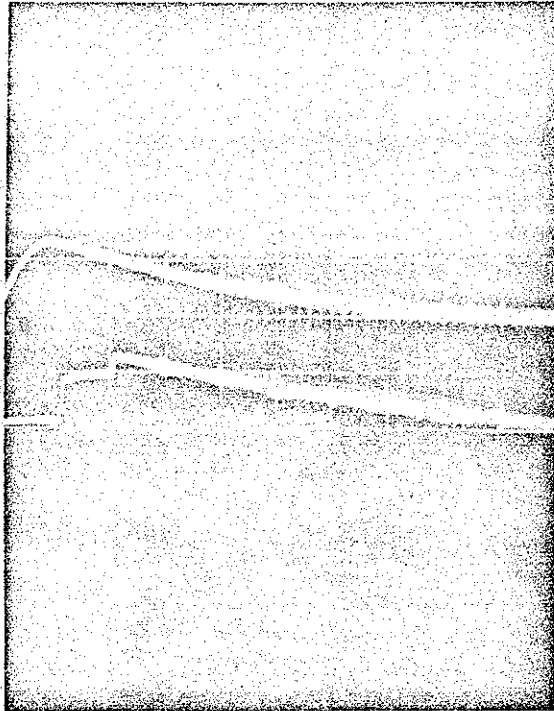


Fig. 21(a): Crowbar and Interruption
at 2.2 msec

IND-1 at 370 j (1 kv - 800 μ f)

SSI-2 fired at 9 kv - 6 μ f

Pressure: 10^{-4} mm of Hg

Load: $R = .160 \Omega$, $L = 5.8 \mu$ h

Upper: Current, IND-1

.05 v/cm

2 msec/cm

RC = 100 msec

Lower: Voltage across Load + SSI-2

50 v/cm

2 msec/cm

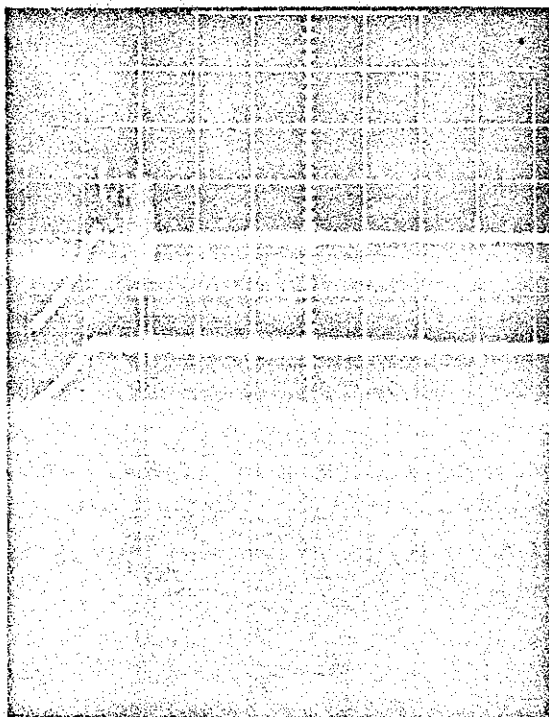


Fig. 21(b): Current through SSI-2 and IND-1

Upper: dI/dt through SSI-2 (Rogowski loop)

10 mv/cm

2 msec/cm

Lower: dI/dt through IND-1 (Rogowski loop)

10 mv/cm

2 msec/cm

Rogowski Loop Constant 24.5×10^6 amp/v sec

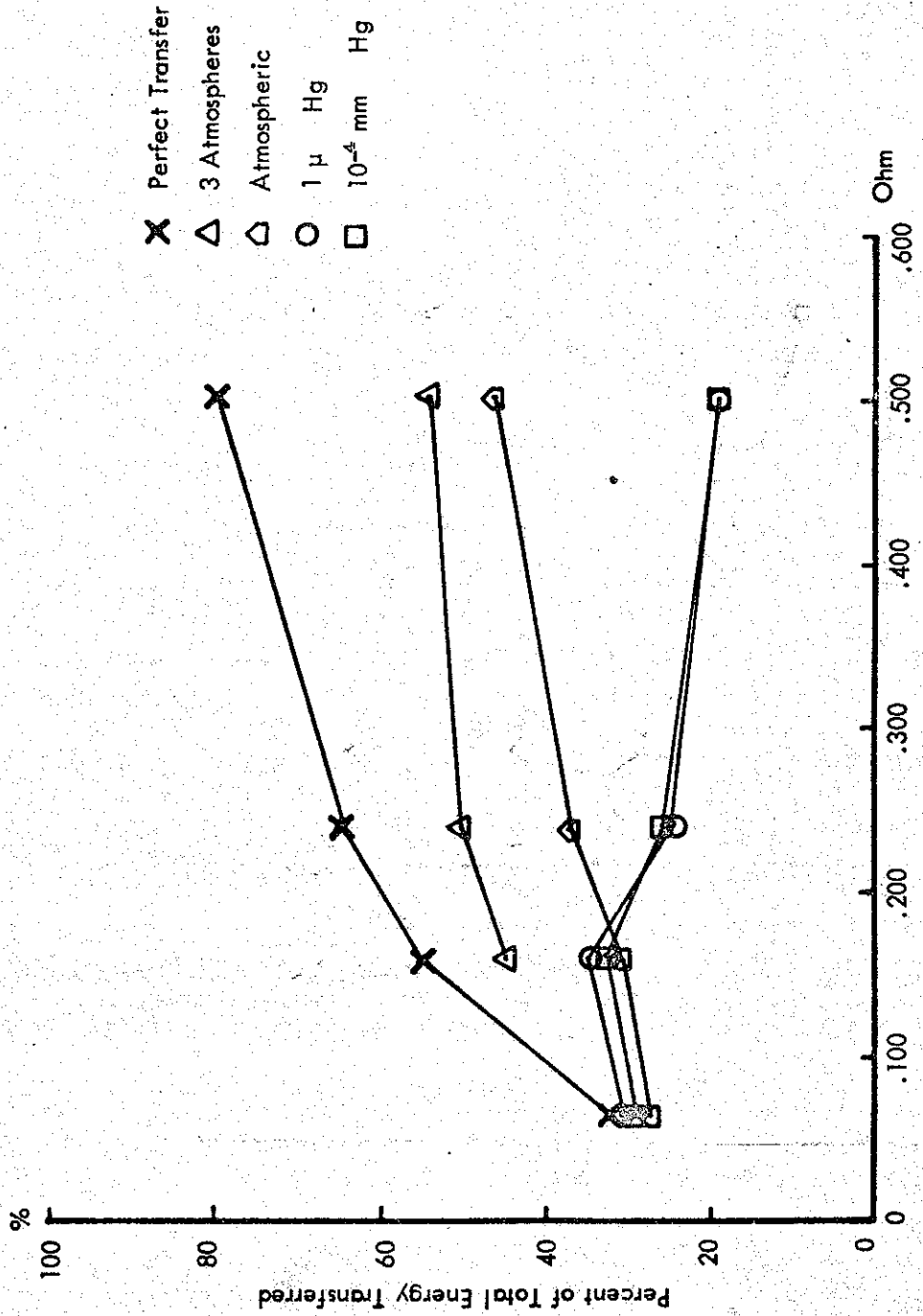


Fig. 22(a): SSI-2 % of Total Energy Transferred vs Resistance

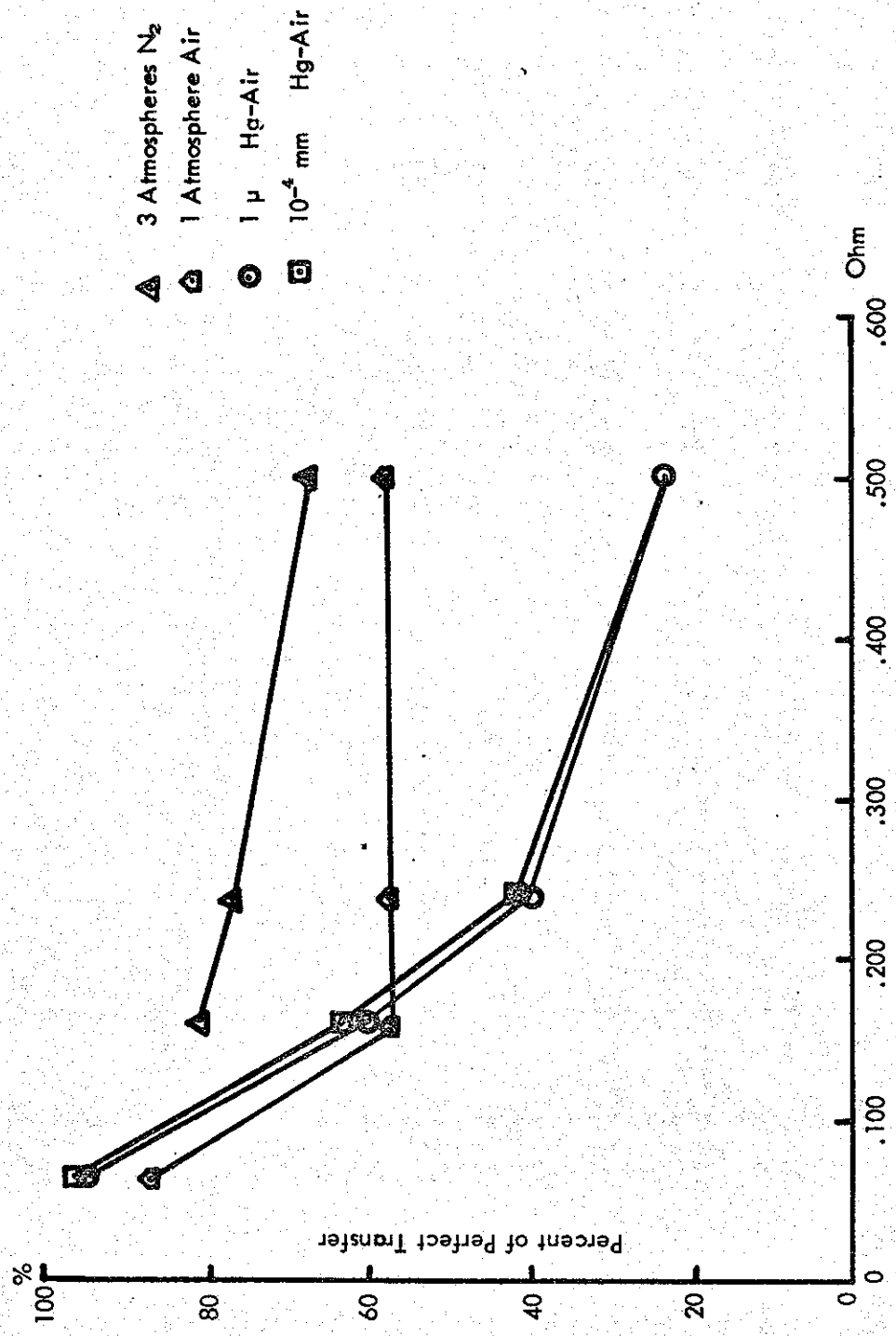


Fig. 22(b): SSI-2 % of Perfect Transfer vs Resistance

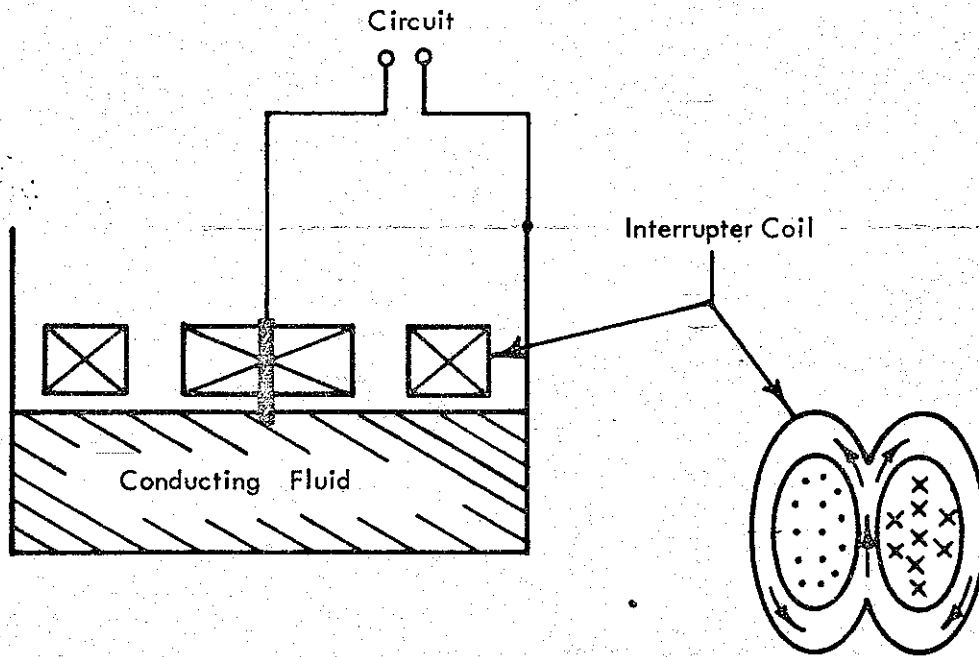


Fig. 23

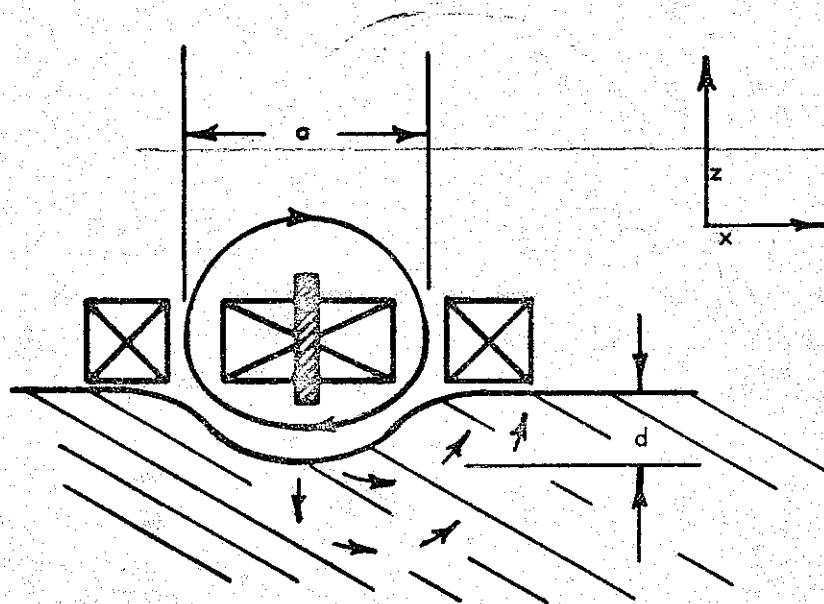


Fig. 24

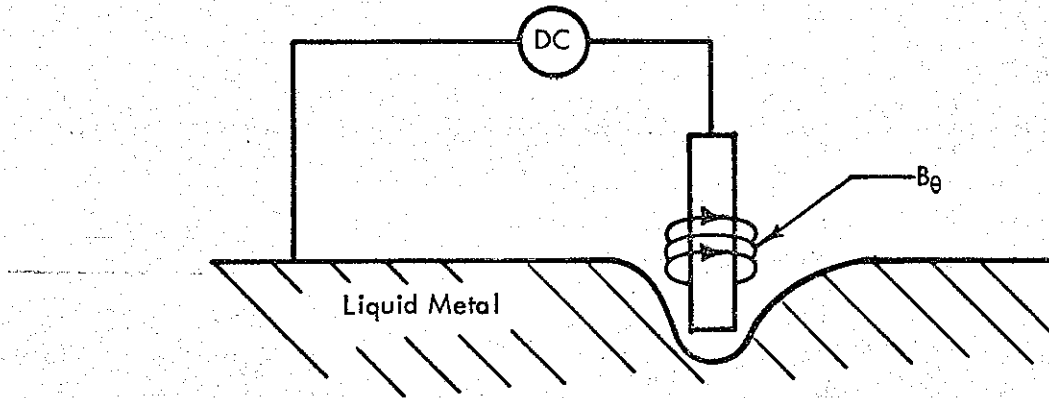


Fig. 25

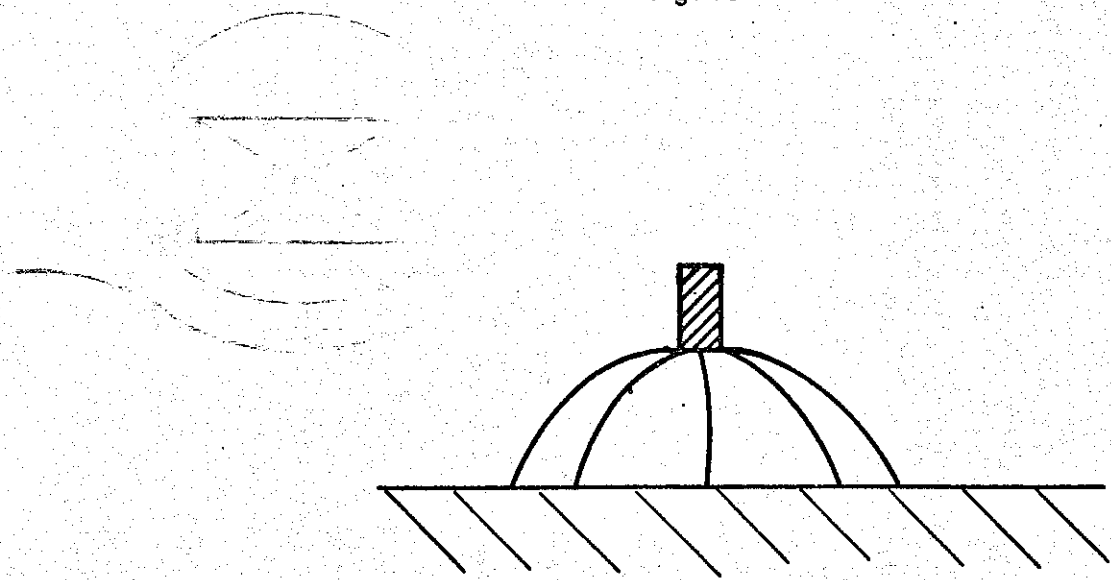


Fig. 26(a)

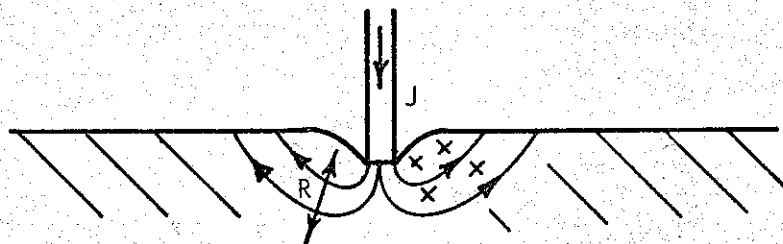


Fig. 26(b)

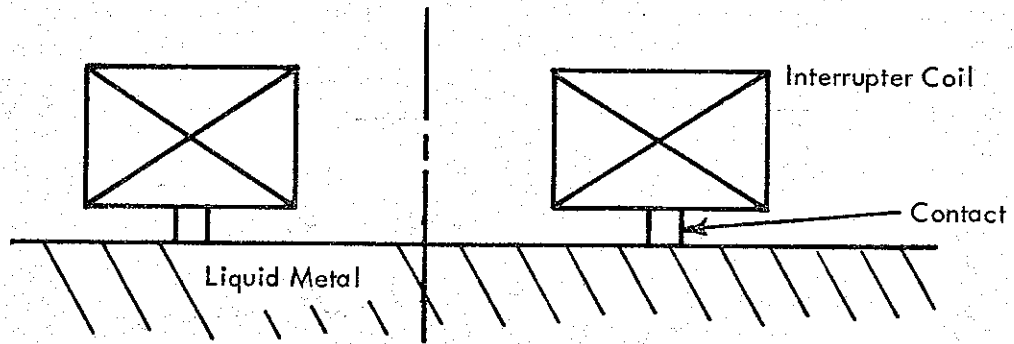


Fig. 27(a)

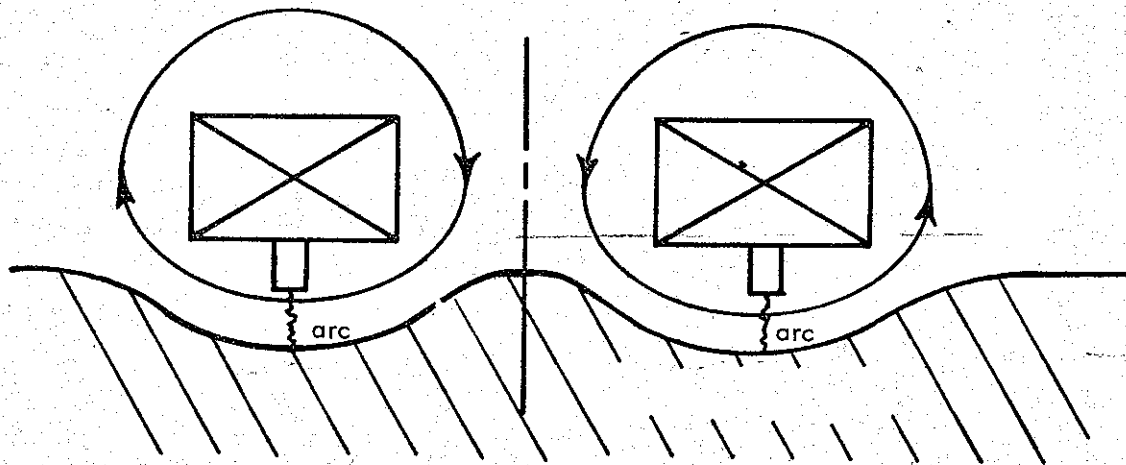


Fig. 27(b)

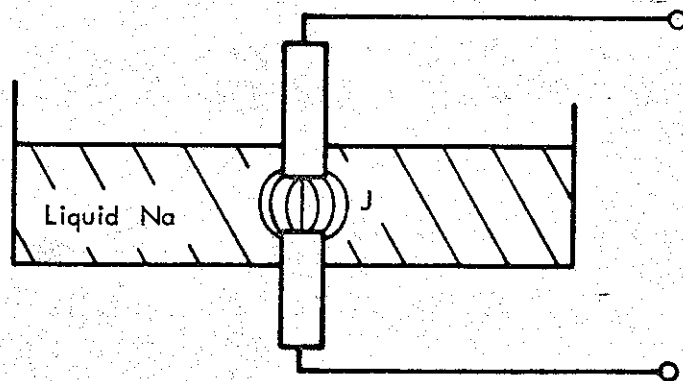


Fig. 28

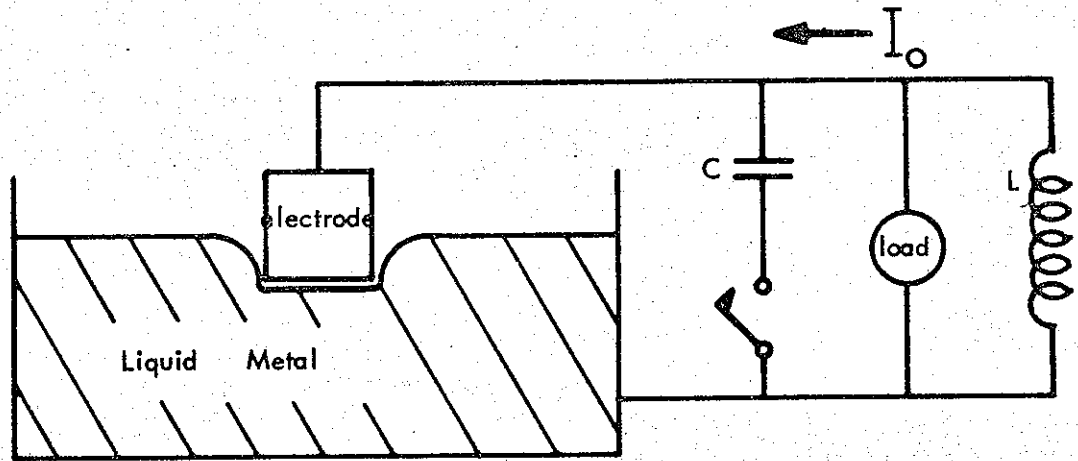


Fig. 29

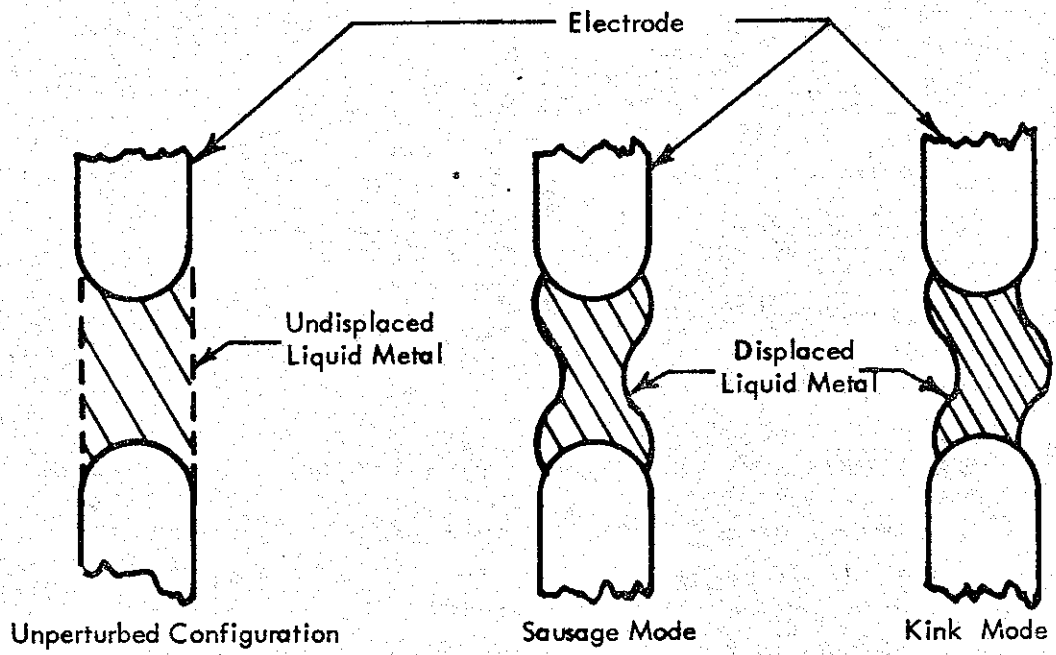


Fig. 30

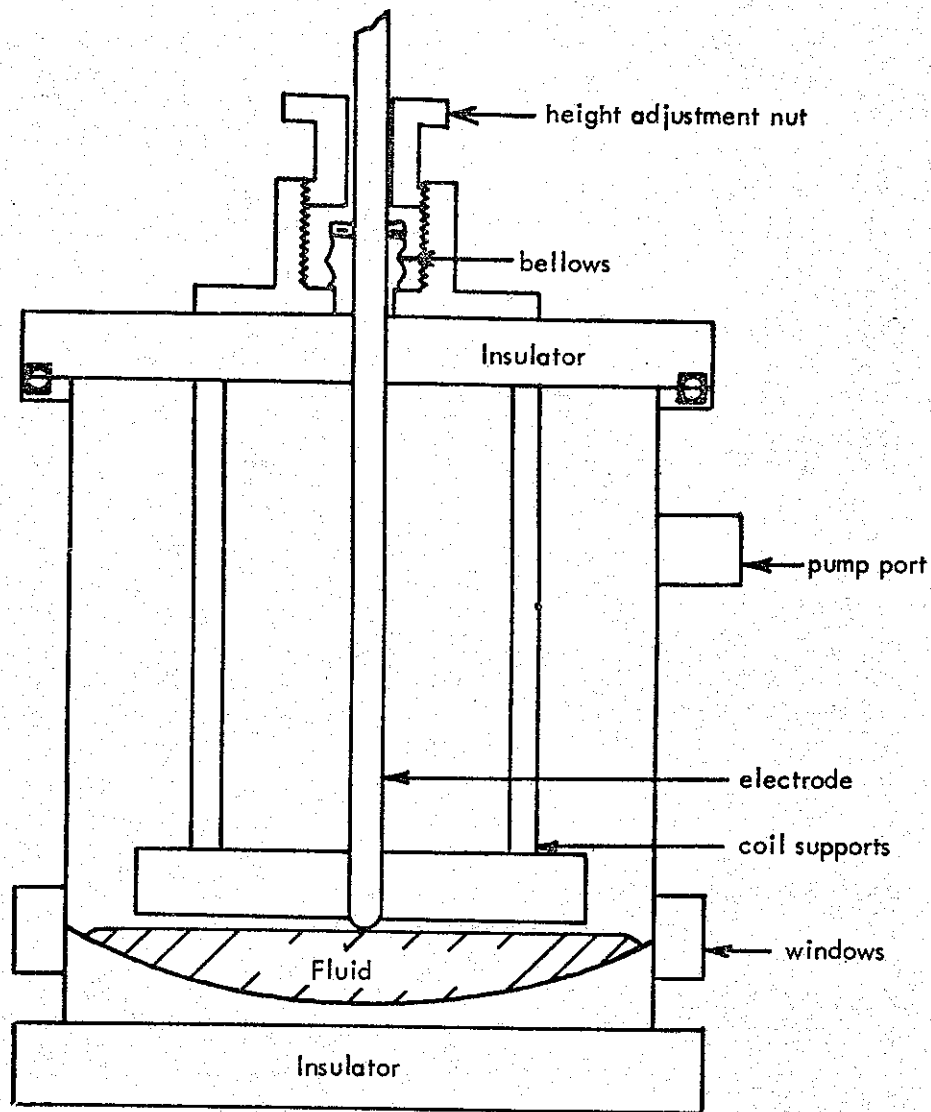


Fig. 31: Liquid Mercury MSI-1 Interrupter

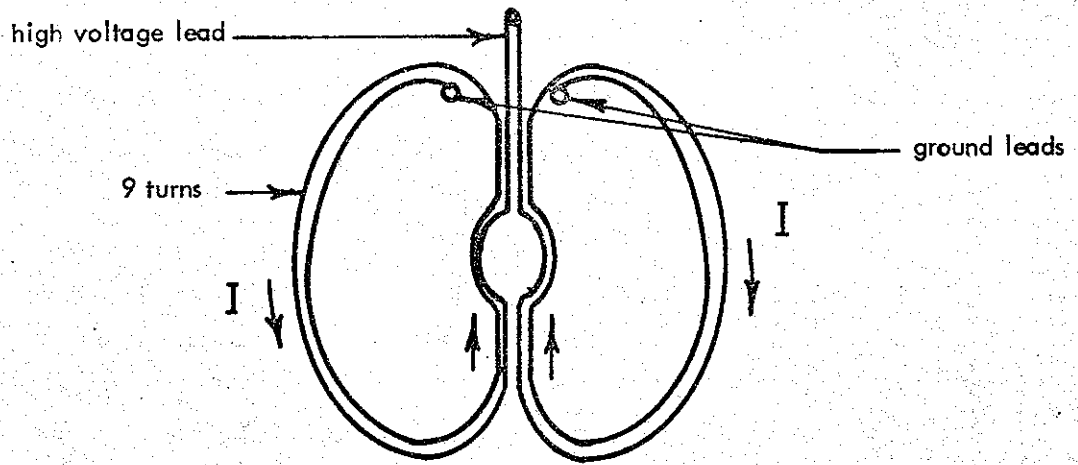


Fig. 32(a): Kidney-Shaped Coil Configuration

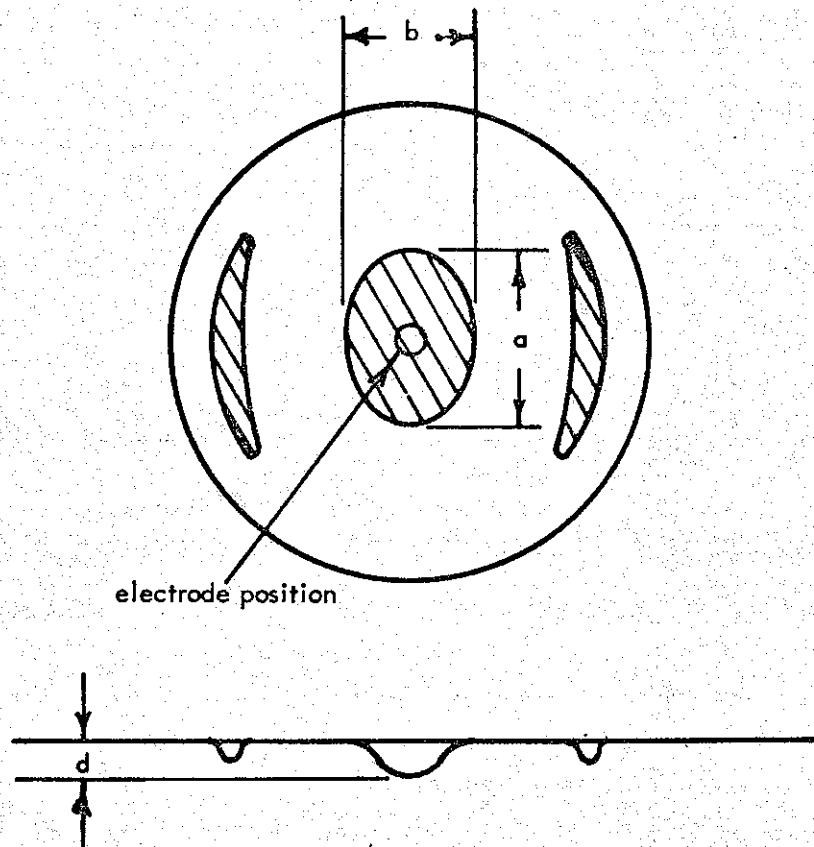


Fig. 32(b): Deformation of Aluminum Foil by Kidney-Shaped Coil

Fig. 33(d): H_z at Coil Surface (through coil center)

$$E = 1.6 \text{ j } (36 \mu\text{f} - 300 \text{ v}) (z = 0.1'')$$

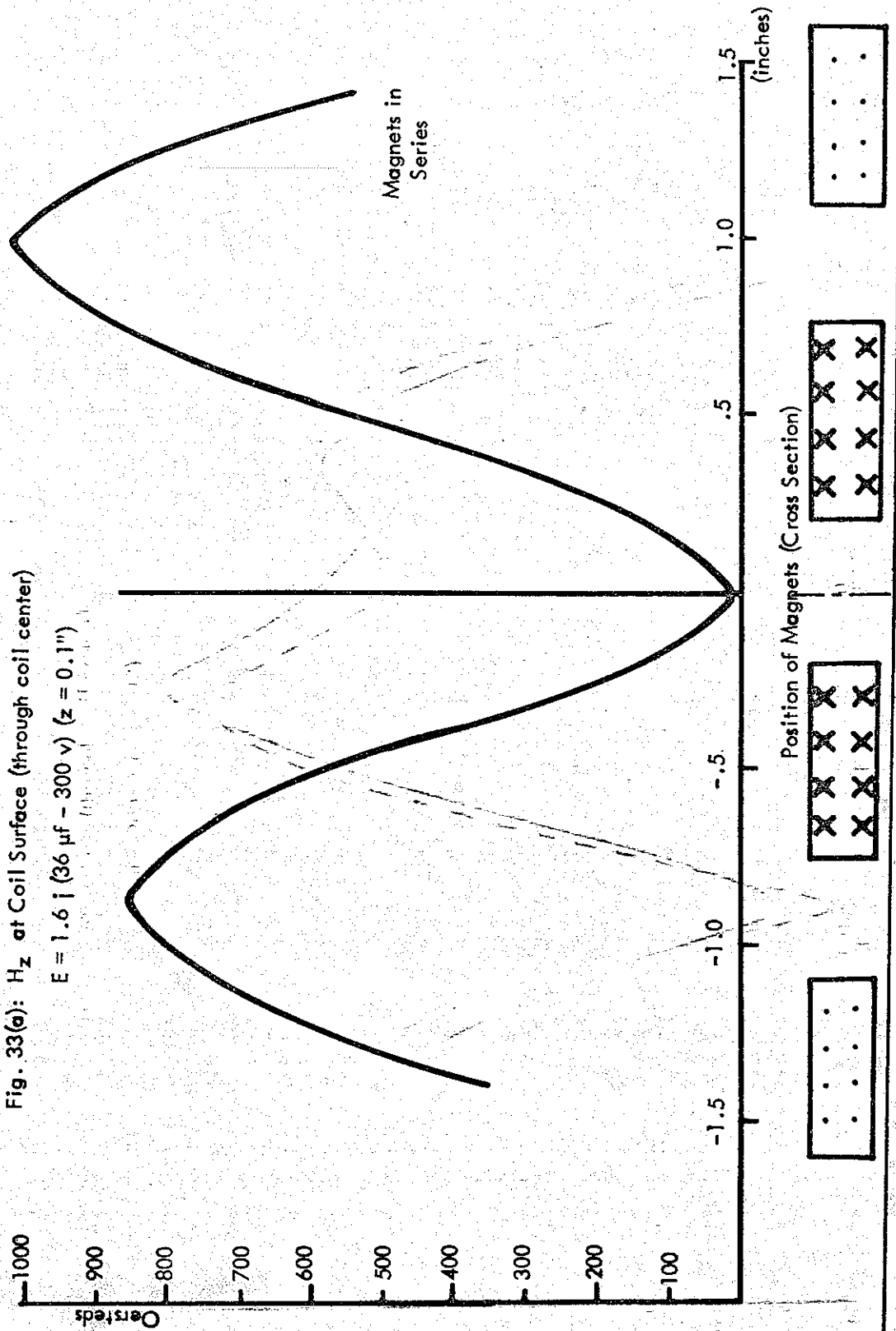
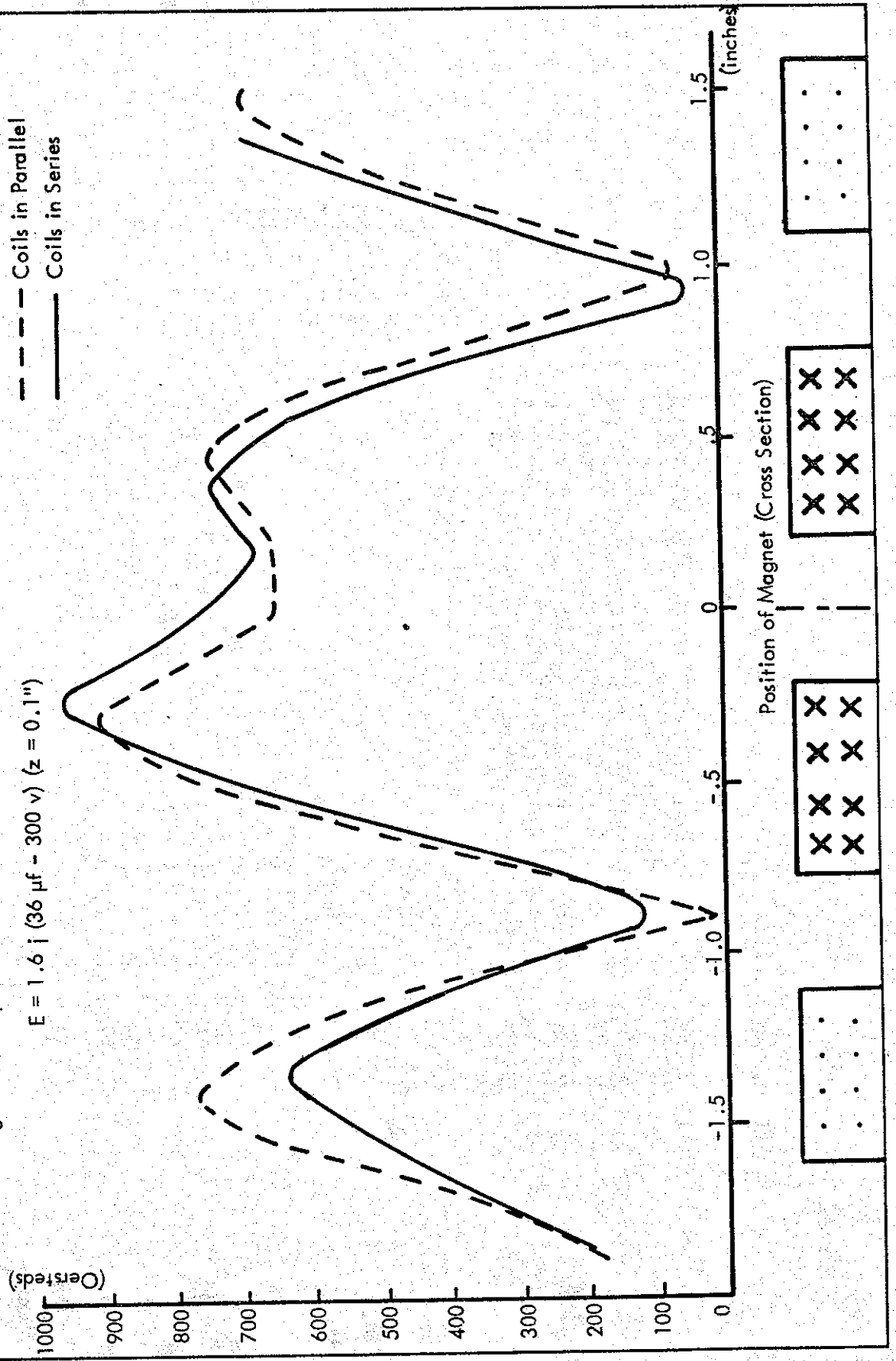
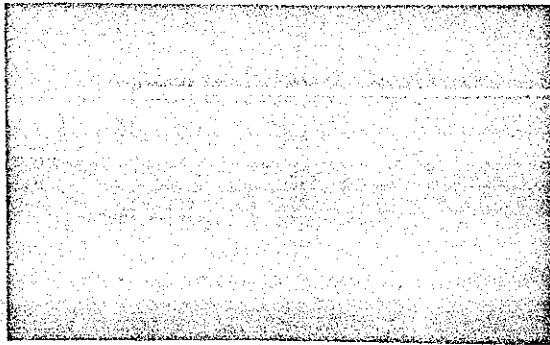


Fig. 33(b): H_r at Coil Surface (through coil center)

$E = 1.6 \text{ j } (36 \mu\text{f} - 300 \text{ v}) (z = 0.1\text{'})$

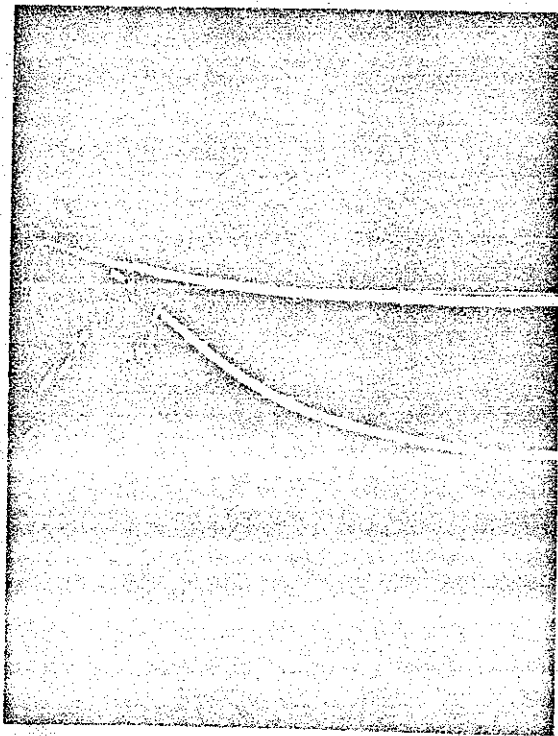




20 $\mu\text{sec}/\text{cm}$
5 v/cm

Fig. 34: MSI-1 Fired at 20 μsec

Breaking begins at 8 μsec after firing and
is completed at 24 μsec after trigger.



Upper: Current in IND-1 by
Integration from One Turn
Loop in Coil Center

.05 v/cm
5 msec/cm
RC = .5 sec

Lower: Voltage, Load and
MSI-2

20 v/cm
5 msec/cm

Fig. 36: 5 Atmospheres of N_2 , .074 Ω Load
Maximum Voltage 65 v

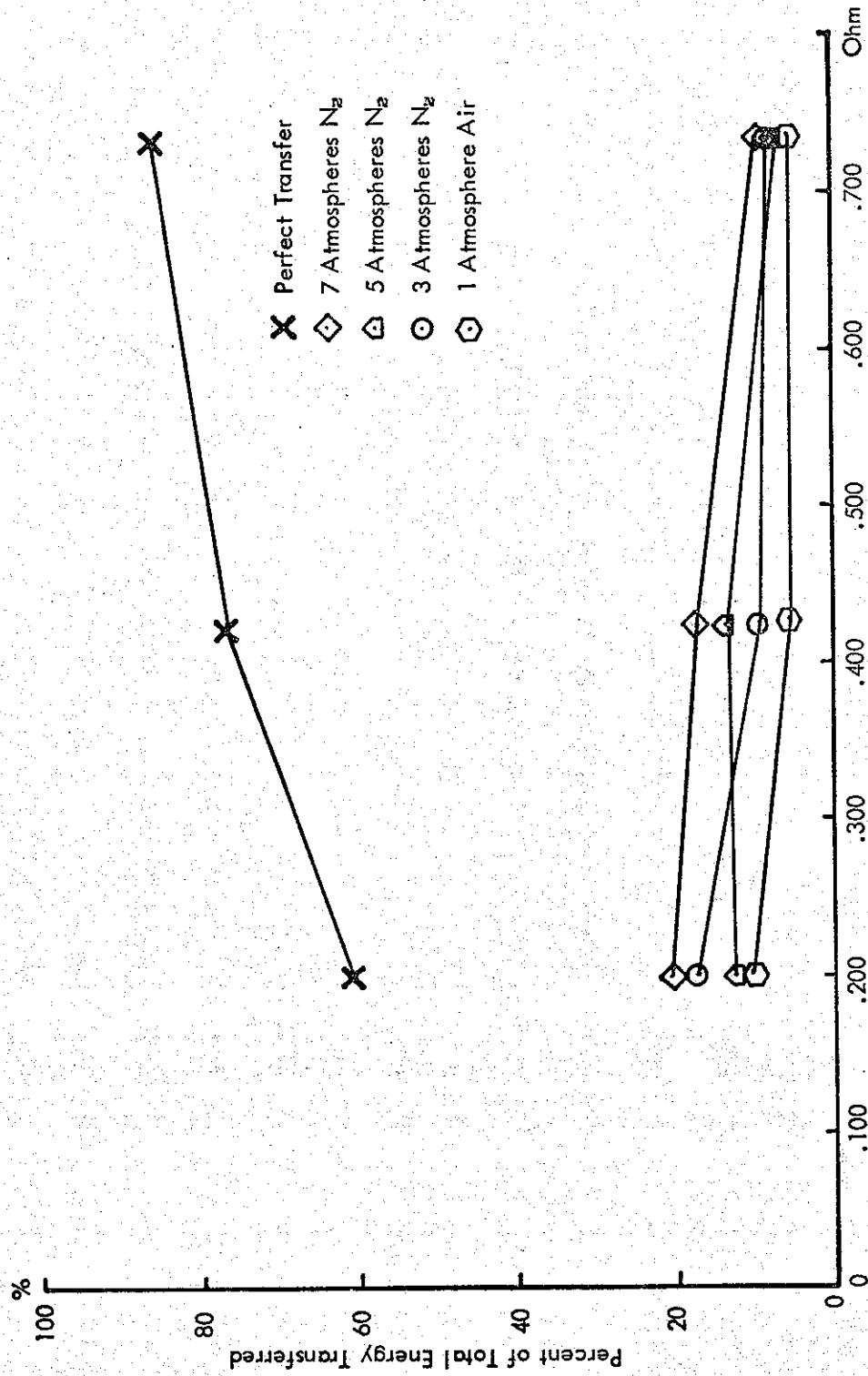


Fig. 35(a): MS1-1 % of Total Energy Transferred vs Load Resistance
(Magnet-Driven Mode)